NASA CR-173,254

NASA-CR-173254
19840008789

A Reproduced Copy

OF

NASA CR-173,254

Reproduced for NASA

by the

NASA Scientific and Technical Information Facility

FFNo 672 Aug 65

CRA

NAG-1-226

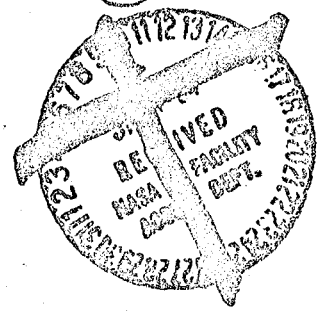

THREE-DIMENSIONAL UNSTEADY EULER EQUATION SOLUTIONS USING FLUX VECTOR SPLITTING

David L. Whitfield
Department of Aerospace Engineering
Mississippi State University
Mississippi State, MS 39762

December 1983

N84-16857#

FOREWARD

This research was sponsored by the NASA Langley Research Center under Grant NASA NAG-1-226 with Dr. Frank Thames as Technical Monitor, and the United States Air Force, Eglin Air Force Base, Florida under Grant F08635-82-K-0409 with Dr. Larry Lijewski as Technical Officer. The support of NASA and the Air Force, as well as technical interactions with Drs. Thames and Lijewski, is gratefully acknowledged.

ABSTRACT

A method for numerically solving the three-dimensional unsteady Euler equations using flux vector splitting is developed. The equations are cast in curvilinear coordinates and a finite volume discretization is used. An explicit upwind second-order predictor-corrector scheme is used to solve the discretized equations. The scheme is stable for a CFL number of 2 and local time stepping is used to accelerate convergence for steady-state problems. Characteristic variable boundary conditions are developed and used in the far field and at surfaces. No additional dissipation terms are included in the scheme. Numerical results are compared with results from an existing three-dimensional Euler code and experimental data.

I. INTRODUCTION

In support of NASA's interest in the use of prop-fans as a propulsion device, a computational method was recently developed for numerically solving the flowfield about a swept, tapered, supercritical wing with a propeller producing thrust and swirl (Ref. 1). The equations solved were essentially Euler equations with body force terms included to simulate the propeller. The Euler solver used was an extension of the method of Jameson, et. al. (Refs. 2 and 3) referred to as FL057. Although good agreement was obtained with experimental data (Ref. 1), some difficulty in convergence, particularly the energy equation, was encountered using the FL057 central-difference scheme. Recently, convergence difficulties were also reported by Swafford (Ref. 4) in solving a set of hyperbolic equations with source terms (which can be considered similar to the force terms included in the Euler equations in Ref. 1) using a similar central-difference scheme. An upwind scheme eliminated the convergence problems in Ref. 4. Moreover, any additional smoothing added to the upwind scheme was found to be detrimental with regard to convergence. (Additional smoothing was found to always be necessary in using the central-difference scheme in Ref. 4.) Therefore, it seemed appropriate to consider an upwind scheme for solving the three-dimensional Euler equations.

The flux-vector-split form of the equations used is developed in the following section. The motivation and background of using splitting is given in the literature (see, for example, Steger and Warming (Ref. 5)) and is not repeated here. Moreover, many of the matrices needed are given in the literature (see Refs. 6 and 7); however, all equations

and matrices needed are developed and included in Section II for clarity and completeness. Formulation of the equations for numerical solution and the algorithm used to solve the discretized equations are discussed in Section III. The characteristic variable boundary conditions used in the farfield and at surfaces are developed in Section IV. Numerical results, including comparisons with FL057 solutions and experimental data, are presented and discussed in Section V.

II. SPLITTING

The conservation law vector form of the Euler equations in Cartesian coordinates x,y, and z are

$$\frac{\partial \bar{q}}{\partial t} + \frac{\partial f}{\partial x} + \frac{\partial g}{\partial y} + \frac{\partial h}{\partial z} = 0 \tag{2.1}$$

where

$$\bar{q} = [\rho,\ \rho u,\ \rho v,\ \rho w,\ e]^T$$

$$f = [\rho u,\ \rho u^2 + p,\ \rho uv,\ \rho uw,\ u(e + p)]^T$$

$$g = [\rho v,\ \rho uv,\ \rho v^2 + p,\ \rho vw,\ v(e + p)]^T$$

$$h = [\rho w,\ \rho uw,\ \rho vw,\ \rho w^2 + p,\ w(e + p)]^T$$

$$p = (\gamma - 1)[e - \tfrac{1}{2}\rho(u^2 + v^2 + w^2)]$$

Using curvilinear coordinates defined as

$$\xi = \xi(x,y,z)$$

$$\eta = \eta(x,y,z)$$

$$\zeta = \zeta(x,y,z)$$

$$\tau = t$$

it is straightforward to transform Eq. (2.1) to

$$\frac{\partial Q}{\partial \tau} + \frac{\partial F}{\partial \xi} + \frac{\partial G}{\partial \eta} + \frac{\partial H}{\partial \zeta} = 0 \tag{2.2}$$

where

$$Q = J[\rho,\ \rho u,\ \rho v,\ \rho w,\ e]^T$$

$$F = J[\rho U,\ \rho uU + \xi_x p,\ \rho vU + \xi_y p,\ \rho wU + \xi_z p,\ U(e + p)]^T$$

$$G = J[\rho V,\ \rho uV + \eta_x p,\ \rho vV + \eta_y p,\ \rho wV + \eta_z p,\ V(e + p)]^T$$

$$H = J[\rho W,\ \rho uW + \zeta_x p,\ \rho vW + \zeta_y p,\ \rho wW + \zeta_z p,\ W(e + p)]^T$$

$$J = x_\xi(y_\eta z_\zeta - z_\eta y_\zeta) - y_\xi(x_\eta z_\zeta - z_\eta x_\zeta) + z_\xi(x_\eta y_\zeta - y_\eta x_\zeta)$$

$$\xi_x = J^{-1}(y_\eta z_\zeta - z_\eta y_\zeta)$$

$$\eta_x = J^{-1}(z_\xi y_\zeta - y_\xi z_\zeta)$$

$$\zeta_x = J^{-1}(y_\xi z_\eta - z_\xi y_\eta)$$

$$\xi_y = J^{-1}(z_\eta x_\zeta - x_\eta z_\zeta)$$

$$\eta_y = J^{-1}(x_\xi z_\zeta - z_\xi x_\zeta)$$

$$\zeta_y = J^{-1}(z_\xi x_\eta - x_\xi z_\eta)$$

$$\xi_z = J^{-1}(x_\eta y_\zeta - y_\eta x_\zeta)$$

$$\eta_z = J^{-1}(y_\xi x_\zeta - x_\xi y_\zeta)$$

$$\zeta_z = J^{-1}(x_\xi y_\eta - y_\xi x_\eta)$$

$$U = \xi_x u + \xi_y v + \xi_z w$$

$$V = \eta_x u + \eta_y v + \eta_z w$$

$$W = \zeta_x u + \zeta_y v + \zeta_z w$$

The strong conservation law of the Euler equations in curvilinear coordinates (Eq. (2.2)) can be written in the quasilinear form

$$\frac{\partial Q}{\partial \tau} + A\frac{\partial Q}{\partial \xi} + B\frac{\partial Q}{\partial \eta} + C\frac{\partial Q}{\partial \zeta} = 0 \qquad (2.3)$$

where the matrices A, B, and C are given by

$$A = \frac{\partial F}{\partial Q}$$

$$B = \frac{\partial G}{\partial Q}$$

$$C = \frac{\partial H}{\partial Q}$$

Carrying out these operations, one obtains a matrix $\bar{\bar{K}}$

$$\bar{\bar{K}} = \begin{bmatrix} 0 & k_x & k_y & k_z & 0 \\ k_x\phi - u\theta_k & k_x(2-\gamma)u + \theta_k & k_y u - k_x(\gamma-1)v & k_z u - k_x(\gamma-1)w & k_x(\gamma-1) \\ k_y\phi - v\theta_k & k_x v - k_y(\gamma-1)u & k_y(2-\gamma)v + \theta_k & k_z v - k_y(\gamma-1)w & k_y(\gamma-1) \\ k_z\phi - w\theta_k & k_x w - k_z(\gamma-1)u & k_y w - k_z(\gamma-1)v & k_z(2-\gamma)w + \theta_k & k_z(\gamma-1) \\ (2\phi - \frac{\gamma e}{\rho})\theta_k & k_x(\frac{\gamma e}{\rho} - \phi) - (\gamma-1)u\theta_k & k_y(\frac{\gamma e}{\rho} - \phi) - (\gamma-1)v\theta_k & k_z(\frac{\gamma e}{\rho} - \phi) - (\gamma-1)w\theta_k & \gamma\theta_k \end{bmatrix} \qquad (2.4)$$

where

$$\phi = \frac{\gamma-1}{2}(u^2 + v^2 + w^2)$$

$$\theta_k = k_x u + k_y v + k_z w$$

and matrices A, B, and C are given by the matrix $\bar{\bar{K}}$ depending on whether

k in Eq. (2.4) is ξ, η, or ζ. That is

$$\begin{aligned} \bar{K} &= A \quad \text{for } k = \xi \\ \bar{K} &= B \quad \text{for } k = \eta \\ \bar{K} &= C \quad \text{for } k = \zeta \end{aligned} \tag{2.5}$$

The eigensystem of the matrices A, B, and C is important to achieve the intented splitting. However, there are few zero elements in Eq. (2.4) and the eigenvalues of A, B, and C are difficult to determine using Eq. (2.4) directly. Hence, consider the nonconservative vector form of the Euler equations in curvilinear coordinates

$$\frac{\partial q}{\partial \tau} + a \frac{\partial q}{\partial \xi} + b \frac{\partial q}{\partial \eta} + c \frac{\partial q}{\partial \zeta} = 0 \tag{2.6}$$

where

$$q = J[\rho, u, v, w, p]^T$$

Note that Eq. (2.3) can be written as

$$M \frac{\partial q}{\partial \tau} + AM \frac{\partial q}{\partial \xi} + BM \frac{\partial q}{\partial \eta} + CM \frac{\partial q}{\partial \zeta} = 0 \tag{2.7}$$

where M is the matrix $\frac{\partial Q}{\partial q}$. Multiply Eq. (2.7) on the left by M^{-1} to obtain

$$I \frac{\partial q}{\partial \tau} + M^{-1}AM \frac{\partial q}{\partial \xi} + M^{-1}BM \frac{\partial q}{\partial \eta} + M^{-1}CM \frac{\partial q}{\partial \zeta} = 0$$

where I is the identity matrix. Then from Eqs. (2.6) and (2.7)

$$\begin{aligned} a &= M^{-1}AM \\ b &= M^{-1}BM \\ c &= M^{-1}CM \end{aligned} \tag{2.8}$$

Therefore, the matrix a is similar to A, b is similar to B, and c is similar to C. Because similar matrices have the same eigenvalues (Ref. 8), the eigenvalues of A, B, and C are known by determining the eigenvalues of a, b, and c. The matrices a, b, and c are more simple to handle than matrices A, B, and C because they contain several zero elements as shown below.

The matrices a, b, and c are now determined. The matrix M given by $\frac{\partial Q}{\partial q}$ is

$$M = \begin{bmatrix} 1 & 0 & 0 & 0 & 0 \\ u & \rho & 0 & 0 & 0 \\ v & 0 & \rho & 0 & 0 \\ w & 0 & 0 & \rho & 0 \\ \frac{\phi}{\gamma-1} & \rho u & \rho v & \rho w & \frac{1}{\gamma-1} \end{bmatrix} \qquad (2.9)$$

The inverse of this matrix is

$$M^{-1} = \begin{bmatrix} 1 & 0 & 0 & 0 & 0 \\ -\frac{u}{\rho} & \frac{1}{\rho} & 0 & 0 & 0 \\ -\frac{v}{\rho} & 0 & \frac{1}{\rho} & 0 & 0 \\ -\frac{w}{\rho} & 0 & 0 & \frac{1}{\rho} & 0 \\ \phi & -u(\gamma-1) & -v(\gamma-1) & -w(\gamma-1) & (\gamma-1) \end{bmatrix} \qquad (2.10)$$

Then by Eqs. (2.8) the matrices a, b, and c are given by

$$\kappa = \begin{bmatrix} \theta_k & \rho k_x & \rho k_y & \rho k_z & 0 \\ 0 & \theta_k & 0 & 0 & \frac{k_x}{\rho} \\ 0 & 0 & \theta_k & 0 & \frac{k_y}{\rho} \\ 0 & 0 & 0 & \theta_k & \frac{k_z}{\rho} \\ 0 & k_x\rho c^2 & k_y\rho c^2 & k_z\rho c^2 & \theta_k \end{bmatrix} \tag{2.11}$$

where

$$\begin{aligned} \kappa &= a \quad \text{for } k = \xi \\ \kappa &= b \quad \text{for } k = \eta \\ \kappa &= c \quad \text{for } k = \zeta \end{aligned} \tag{2.12}$$

The c in the ρc^2 terms in Eq. (2.11) is the speed of sound and is not to be confused with the matrix c. The ϕ appearing in Eqs. (2.9) and (2.10) is again

$$\phi = \frac{\gamma-1}{2}(u^2 + v^2 + w^2)$$

just as in Eqs. (2.4).

From Eq. (2.11) the eigenvalues of matrices a, b, and c are easily determined. The eigenvalues are

$$\begin{aligned} \lambda_k^1 &= \lambda_k^2 = \lambda_k^3 = k_x u + k_y v + k_z w = \theta_k \\ \lambda_k^4 &= \theta_k + c|\nabla k| \\ \lambda_k^5 &= \theta_k - c|\nabla k| \end{aligned} \tag{2.13}$$

where λ_k^1, λ_k^2, λ_k^3, λ_k^4, and λ_k^5 are the eigenvalues of a for $k = \xi$, b for $k = \eta$, and c for $k = \zeta$. Correspondingly, the eigenvectors are

$$
\begin{aligned}
x_1 &= [\tilde{k}_x,\ 0,\ \tilde{k}_z,\ -\tilde{k}_y,\ 0]^T \\
x_2 &= [\tilde{k}_y,\ -\tilde{k}_z,\ 0,\ \tilde{k}_x,\ 0]^T \\
x_3 &= [\tilde{k}_z,\ \tilde{k}_y,\ -\tilde{k}_x,\ 0,\ 0]^T \\
x_4 &= \frac{1}{\sqrt{2}}\left[\frac{\rho}{c},\ \tilde{k}_x,\ \tilde{k}_y,\ \tilde{k}_z,\ \rho c\right]^T \\
x_5 &= \frac{1}{\sqrt{2}}\left[\frac{\rho}{c},\ -\tilde{k}_x,\ -\tilde{k}_y,\ -\tilde{k}_z,\ \rho c\right]^T
\end{aligned}
\tag{2.14}
$$

where

$$
\begin{aligned}
\tilde{k}_x &= \frac{k_x}{|\nabla k|} = \frac{k_x}{(k_x^2 + k_y^2 + k_z^2)^{1/2}} \\
\tilde{k}_y &= \frac{k_y}{|\nabla k|} \\
\tilde{k}_z &= \frac{k_z}{|\nabla k|}
\end{aligned}
\tag{2.15}
$$

Sufficient equations have now been developed to carry out the splitting. The integral conservation law form of the Euler equations will be formulated and discretized for numerical solution in the following section. This formulation requires evaluation of the vectors F, G, and H at faces of the finite volumes. By splitting the vectors F, G, and H into the sum of separate vectors, each having an eigenvalue as a coefficient, the evaluation of each separate vector by extrapolating from the appropriate direction indicated by the sign of its eigenvalue can be carried out.

The vectors F, G, and H are homogeneous functions of degree one in Q; therefore, by Euler's Theorem (Ref. 9)

$$K = \bar{K}Q \tag{2.16}$$

where $K = F$ and $\bar{K} = A$ for $k = \xi$, $K = G$ and $\bar{K} = B$ for $k = \eta$, and $K = H$ and $\bar{K} = C$ for $k = \zeta$. The matrices $\bar{K}$ can be written

$$\bar{K} = T_k \Lambda_k T_k^{-1} \tag{2.17}$$

where Λ_k is the diagonal matrix whose diagonal elements are the eigenvalues of κ (or, also, $\bar{K}$) given by Eq. (2.13) The matrices κ given by Eq. (2.12) can be written

$$\kappa = P_k \Lambda_k P_k^{-1} \tag{2.18}$$

where the columns of P_k are the eigenvectors of κ corresponding to the respective eigenvalues. From Eqs. (2.8)

$$\bar{K} = M\kappa M^{-1} \tag{2.19}$$

Using Eq. (2.18) in Eq. (2.19)

$$\bar{K} = MP_k \Lambda_k P_k^{-1} M^{-1} \tag{2.20}$$

Then from Eqs. (2.17) and (2.20)

$$T_k = MP_k \tag{2.21a}$$

$$T_k^{-1} = P_k^{-1} M^{-1} \tag{2.21b}$$

The matrices M and M^{-1} are given by Eqs. (2.9) and (2.10). The matrix P_k is

$$P_k = \begin{bmatrix} \tilde{k}_x & \tilde{k}_y & \tilde{k}_z & \alpha & \alpha \\ 0 & -\tilde{k}_z & \tilde{k}_y & \frac{\tilde{k}_x}{\sqrt{2}} & -\frac{\tilde{k}_x}{\sqrt{2}} \\ \tilde{k}_z & 0 & -\tilde{k}_x & \frac{\tilde{k}_y}{\sqrt{2}} & -\frac{\tilde{k}_y}{\sqrt{2}} \\ -\tilde{k}_y & \tilde{k}_x & 0 & \frac{\tilde{k}_z}{\sqrt{2}} & -\frac{\tilde{k}_z}{\sqrt{2}} \\ 0 & 0 & 0 & \alpha c^2 & \alpha c^2 \end{bmatrix} \qquad (2.22)$$

where

$$\alpha = \frac{\rho}{\sqrt{2}\, c}$$

Rather than invert P_k directly, the matrix P_k^{-1} can be determined easily from the left eigenvectors of κ. The left eigenvectors of κ are the rows of P_k^{-1}, i.e.

$$P_k^{-1} = \begin{bmatrix} \tilde{k}_x & 0 & \tilde{k}_z & -\tilde{k}_y & -\frac{\tilde{k}_x}{c^2} \\ \tilde{k}_y & -\tilde{k}_z & 0 & \tilde{k}_x & -\frac{\tilde{k}_y}{c^2} \\ \tilde{k}_z & \tilde{k}_y & -\tilde{k}_x & 0 & -\frac{\tilde{k}_z}{c^2} \\ 0 & \frac{\tilde{k}_x}{\sqrt{2}} & \frac{\tilde{k}_y}{\sqrt{2}} & \frac{\tilde{k}_z}{\sqrt{2}} & \beta \\ 0 & -\frac{\tilde{k}_x}{\sqrt{2}} & -\frac{\tilde{k}_y}{\sqrt{2}} & -\frac{\tilde{k}_z}{\sqrt{2}} & \beta \end{bmatrix} \qquad (2.23)$$

where

$$\beta = \frac{1}{\sqrt{2}\ \rho c}$$

The matrices T_k and T_k^{-1} can now be determined using Eqs. (2.21). These matrices are

$$T_k = \begin{bmatrix} \tilde{k}_x & \tilde{k}_y & \tilde{k}_z \\ u\tilde{k}_x & u\tilde{k}_y - \rho\tilde{k}_z & u\tilde{k}_z + \rho\tilde{k}_y \\ v\tilde{k}_x + \rho\tilde{k}_z & v\tilde{k}_y & v\tilde{k}_z - \rho\tilde{k}_x \\ w\tilde{k}_x - \rho\tilde{k}_y & w\tilde{k}_y + \rho\tilde{k}_x & w\tilde{k}_z \\ \frac{\phi}{\gamma-1}\tilde{k}_x + \rho(v\tilde{k}_z - w\tilde{k}_y) & \frac{\phi}{\gamma-1}\tilde{k}_y + \rho(w\tilde{k}_x - u\tilde{k}_z) & \frac{\phi}{\gamma-1}\tilde{k}_z + \rho(u\tilde{k}_y - v\tilde{k}_x) \end{bmatrix}$$

$$\begin{bmatrix} \alpha & \alpha \\ \alpha(u + c\tilde{k}_x) & \alpha(u - c\tilde{k}_x) \\ \alpha(v + c\tilde{k}_y) & \alpha(v - c\tilde{k}_y) \\ \alpha(w + c\tilde{k}_z) & \alpha(w - c\tilde{k}_z) \\ \alpha(\frac{\phi+c^2}{\gamma-1} + c\tilde{\theta}_k) & \alpha(\frac{\phi+c^2}{\gamma-1} - c\tilde{\theta}_k) \end{bmatrix} \qquad (2.24a)$$

$$T_k^{-1} = \begin{bmatrix} \tilde{k}_x\left(1-\frac{\phi}{c^2}\right)+\frac{1}{\rho}(w\tilde{k}_y-v\tilde{k}_z) & \tilde{k}_x\frac{u(\gamma-1)}{c^2} & \tilde{k}_z\frac{1}{\rho}+\tilde{k}_x\frac{v(\gamma-1)}{c^2} \\ \tilde{k}_y\left(1-\frac{\phi}{c^2}\right)+\frac{1}{\rho}(v\tilde{k}_x-u\tilde{k}_z) & -\tilde{k}_z\frac{1}{\rho}+\tilde{k}_y\frac{u(\gamma-1)}{c^2} & \tilde{k}_y\frac{v(\gamma-1)}{c^2} \\ \tilde{k}_z\left(1-\frac{\phi}{c^2}\right)+\frac{1}{\rho}(v\tilde{k}_x-u\tilde{k}_y) & \tilde{k}_y\frac{1}{\rho}+\tilde{k}_z\frac{u(\gamma-1)}{c^2} & -\tilde{k}_x\frac{1}{\rho}+\tilde{k}_z\frac{v(\gamma-1)}{c^2} \\ \beta(\phi-c\theta_k) & \beta[c\tilde{k}_x-u(\gamma-1)] & \beta[c\tilde{k}_y-v(\gamma-1)] \\ \beta(\phi+c\theta_k) & -\beta[c\tilde{k}_x+u(\gamma-1)] & -\beta[c\tilde{k}_y+v(\gamma-1)] \end{bmatrix}$$

$$\begin{bmatrix} -\tilde{k}_y\frac{1}{\rho}+\tilde{k}_x\frac{w(\gamma-1)}{c^2} & -\tilde{k}_x\frac{\gamma-1}{c^2} \\ \tilde{k}_x\frac{1}{\rho}+\tilde{k}_y\frac{w(\gamma-1)}{c^2} & -\tilde{k}_y\frac{\gamma-1}{c^2} \\ \tilde{k}_z\frac{w(\gamma-1)}{c^2} & -\tilde{k}_z\frac{\gamma-1}{c^2} \\ \beta[c\tilde{k}_z-w(\gamma-1)] & \beta(\gamma-1) \\ -\beta[c\tilde{k}_z+w(\gamma-1)] & \beta(\gamma-1) \end{bmatrix} \qquad (2.24b)$$

where

$$\phi = \frac{\gamma-1}{2}(u^2+v^2+w^2)$$

$$\tilde{\theta}_k = \tilde{k}_x u + \tilde{k}_y v + \tilde{k}_z w$$

$$\alpha = \frac{\rho}{\sqrt{2}\,c}$$

$$\beta = \frac{1}{\sqrt{2}\,\rho c}$$

Using Eqs. (2.16) and (2.17)

$$K = T_k \Lambda_k T_k^{-1} Q \qquad (2.25)$$

The diagonal matrix

$$\Lambda_k = \begin{bmatrix} \lambda_k^1 & 0 & 0 & 0 & 0 \\ 0 & \lambda_k^2 & 0 & 0 & 0 \\ 0 & 0 & \lambda_k^3 & 0 & 0 \\ 0 & 0 & 0 & \lambda_k^4 & 0 \\ 0 & 0 & 0 & 0 & \lambda_k^5 \end{bmatrix} \tag{2.26}$$

can be written

$$\Lambda_k = \lambda_k^1 I_{1,2,3} + \lambda_k^4 I_4 + \lambda_k^5 I_5 \tag{2.27}$$

where $I_{1,2,3}$ is a matrix which has unity as the first three diagonal elements and all other elements zero, I_4 has unity as the fourth diagonal element and all other elements zero, and I_5 has unity as the fifth diagonal element and all other elements zero. Note that only three terms are needed on the right hand side of Eq. (2.27) instead of five because the first three eigenvalues are the same as shown by Eqs. (2.13). Using Eqs. (2.25) and (2.27), the split form of K is

$$K = \lambda_k^1 T_k I_{1,2,3} T_k^{-1} Q + \lambda_k^4 T_k I_4 T_k^{-1} Q + \lambda_k^5 T_k I_5 T_k^{-1} Q \tag{2.28}$$

or

$$K = K_1 + K_2 + K_3$$

where

$$K_1 = \lambda_k^1 T_k I_{1,2,3} T_k^{-1} Q$$

$$K_2 = \lambda_k^4 T_k I_4 T_k^{-1} Q$$

$$K_3 = \lambda_k^5 T_k I_5 T_k^{-1} Q$$

Everything is now available to carry out these operations and determine the split form of the vector K. The operations described by Eq. (2.28) give

$$K = K_1 + K_2 + K_3 \tag{2.29}$$

where

$$K = F \quad \text{for} \quad k = \xi$$

$$K = G \quad \text{for} \quad k = \eta$$

$$K = H \quad \text{for} \quad k = \zeta$$

$$K_1 = \lambda_k^1 J \frac{\gamma-1}{\gamma} \begin{bmatrix} \rho \\ \rho u \\ \rho v \\ \rho w \\ \frac{1}{2}\rho(u^2 + v^2 + w^2) \end{bmatrix}$$

$$K_2 = \lambda_k^4 \frac{J}{2\gamma} \begin{bmatrix} \rho \\ \rho u + \rho c \tilde{k}_x \\ \rho v + \rho c \tilde{k}_y \\ \rho w + \rho c \tilde{k}_z \\ e + p + \rho c \tilde{\theta}_k \end{bmatrix}$$

$$K_3 = \lambda_k^5 \frac{J}{2\gamma} \begin{bmatrix} \rho \\ \rho u - \rho c \tilde{k}_x \\ \rho v - \rho c \tilde{k}_y \\ \rho w - \rho c \tilde{k}_z \\ e + p - \rho c \tilde{\theta}_k \end{bmatrix}$$

$$\lambda_k^1 = \lambda_k^2 = \lambda_k^3 = k_x u + k_y v + k_z w = \theta_k$$

$$\lambda_k^4 = \theta_k + c|\nabla k|$$

$$\lambda_k^5 = \theta_k - c|\nabla k|$$

$$|\nabla k| = (k_x^2 + k_y^2 + k_z^2)^{1/2}$$

$$\tilde{k}_i = \frac{k_i}{|\nabla k|}$$

$$\tilde{\theta}_k = \tilde{k}_x u + \tilde{k}_y v + \tilde{k}_z w$$

This is the same form of the equations as presented by Reklis and Thomas (Ref. 10).

III. ALGORITHM

The discretized integral form of Eq. (2.2) in computational space for a cell with center denoted as i,j,k is (see, for example, Ref. 11)

$$\frac{\Delta Q}{\Delta \tau}\Delta\xi\Delta\eta\Delta\zeta + (F_{i+\frac{1}{2}} - F_{i-\frac{1}{2}})\Delta\eta\Delta\zeta + (G_{j+\frac{1}{2}} - G_{j-\frac{1}{2}})\Delta\xi\Delta\zeta$$

$$+ (H_{k+\frac{1}{2}} - H_{k-\frac{1}{2}})\Delta\xi\Delta\eta = 0 \qquad (3.1)$$

or

$$\frac{\Delta Q}{\Delta \tau} + \frac{\delta F_i}{\Delta \xi} + \frac{\delta G_j}{\Delta \eta} + \frac{\delta H_k}{\Delta \zeta} = 0 \qquad (3.2)$$

The central difference operator notation in Eq. (3.2) indicates the flux vectors are evaluated at cell faces in this finite volume formulation as illustrated in Fig. 1.

The numerical scheme used is a finite volume version of the second-order upwind scheme of Warming and Beam (Ref. 12). The present scheme is an extension of that used by Deese (Ref. 13) for two-dimensional flow. To illustrate this scheme consider the simple model equation

$$\frac{\partial u}{\partial t} + \frac{\partial F(u)}{\partial x} = 0 \qquad (3.3)$$

where $F(u) = au$; and a is a constant taken as greater than zero for illustration. The second-order upwind scheme of Warming and Beam is

$$\bar{u}_i^{n+1} = u_i^n - \Delta t \frac{\nabla F_i^n}{\Delta x} \qquad (3.4a)$$

$$u_i^{n+1} = \tfrac{1}{2}(u_i^n + \bar{u}_i^{n+1}) - \frac{\Delta t}{2}\frac{\nabla^2 F_i^n}{\Delta x} - \frac{\Delta t}{2}\frac{\nabla \bar{F}_i^{n+1}}{\Delta x} \tag{3.4b}$$

where

$$\nabla F_i^n = F_i^n - F_{i-1}^n = F(u_i^n) - F(u_{i-1}^n)$$

and

$$\bar{F}_i^{n+1} = F(\bar{u}_i^{n+1})$$

The finite volume form of Eq. (3.3) corresponding to Eq. (3.2) is

$$\frac{\Delta u}{\Delta t} + \frac{\delta F_i}{\Delta x} = 0 \tag{3.5}$$

By using the one-point upwind extrapolations, u_i for $u_{i+\frac{1}{2}}$ and u_{i-1} for $u_{i-\frac{1}{2}}$, the predictor step for Eq. (3.5) is

$$\bar{u}_i^{n+1} = u_i^n - \frac{a\Delta t}{\Delta x}(u_i^n - u_{i-1}^n) = u_i^n - \Delta t \frac{\nabla F_i^n}{\Delta x} \tag{3.6}$$

which is the same as Eq. (3.4a). By using the two-point upwind extrapolations, $2u_i - u_{i-1}$ for $u_{i+\frac{1}{2}}$ and $2u_{i-1} - u_{i-2}$ for $u_{i-\frac{1}{2}}$, the finite volume corrector step is

$$u_i^{n+1} = u_i^n - \frac{a\Delta t}{2\Delta x}[(2u_i^n - u_{i-1}^n) - (2u_{i-1}^n - u_{i-2}^n) + (\bar{u}_i^{n+1} - \bar{u}_{i-1}^{n+1})]$$

or

$$u_i^{n+1} = u_i^n - \frac{a\Delta t}{2\Delta x}[(u_i^n - 2u_{i-1}^n + u_{i-2}^n) + (u_i^n - u_{i-1}^n)] - \frac{\Delta t}{2}\frac{\nabla \bar{F}_i^{n+1}}{\Delta x} \tag{3.7}$$

Using Eq. (3.4a), Eq. (3.7) can be written

$$u_i^{n+1} = \tfrac{1}{2}(u_i^n + \bar{u}_i^{n+1}) - \frac{\Delta t}{2}\frac{\nabla^2 F_i^n}{\Delta x} - \frac{\Delta t}{2}\frac{\nabla \bar{F}_i^{n+1}}{\Delta x} \tag{3.8}$$

which is the same form as Warming and Beam's corrector step given by Eq. (3.4b). The stability, dissipation, and dispersion analyses of Ref. 12, therefore, are applicable to the present finite volume scheme. In addition, it is not difficult to show that this scheme is also consistent.

The scheme for the complete three-dimensional unsteady equation is:

Predictor:

$$\tilde{Q}^{n+1}_{i,j,k} = Q^{n}_{i,j,k} - \Delta\tau_{i,j,k} \sum_{\ell=1}^{3} [F_\ell(\tilde{Q}^{n}_{i+\frac{1}{2},j,k}) - F_\ell(\tilde{Q}^{n}_{i-\frac{1}{2},j,k}) + G_\ell(\tilde{Q}^{n}_{i,j+\frac{1}{2},k}) - G_\ell(\tilde{Q}^{n}_{i,j-\frac{1}{2},k}) + H_\ell(\tilde{Q}^{n}_{i,j,k+\frac{1}{2}}) - H(\tilde{Q}^{n}_{i,j,k-\frac{1}{2}})] \qquad (3.9)$$

where the subscript ℓ corresponds to one part of the split vector in Eq. (2.29); and

$$\tilde{Q}^{n}_{i+\frac{1}{2},j,k} = Q^{n}_{i,j,k} \quad \text{if the corresponding } \lambda^1_\xi,\ \lambda^4_\xi, \text{ or } \lambda^5_\xi \text{ eigenvalue evaluated at } i+\tfrac{1}{2},j,k \text{ is } > 0$$

$$\tilde{Q}^{n}_{i+\frac{1}{2},j,k} = Q^{n}_{i+1,j,k} \quad \text{if the corresponding } \lambda^1_\xi,\lambda^4_\xi, \text{ or } \lambda^5_\xi \text{ eigenvalue evaluated at } i+\tfrac{1}{2},j,k \text{ is } \leq 0$$

and similarly for $\tilde{Q}^{n}_{i-\frac{1}{2},j,k}$. The same is done for $\tilde{Q}^{n}_{i,j+\frac{1}{2},k}$ and $\tilde{Q}^{n}_{i,j-\frac{1}{2},k}$ except λ^1_η, λ^4_η, and λ^5_η eigenvalues are interrogated; and similarly, for $\tilde{Q}^{n}_{i,j,k+\frac{1}{2}}$ and $\tilde{Q}^{n}_{i,j,k-\frac{1}{2}}$ except λ^1_ζ, λ^4_ζ, and λ^5_ζ eigenvalues are interrogated.

Corrector:

$$Q^{n+1}_{i,j,k} = Q^{n}_{i,j,k} - \frac{\Delta\tau_{i,j,k}}{2} \sum_{\ell=1}^{3} [F_\ell(\hat{Q}^{n}_{i+\frac{1}{2},j,k}) - F_\ell(\hat{Q}^{n}_{i-\frac{1}{2},j,k})$$

$$+ G_\ell(\hat{Q}^{n}_{i,j+\frac{1}{2},k}) - G_\ell(\hat{Q}^{n}_{i,j-\frac{1}{2},k}) + H_\ell(\hat{Q}^{n}_{i,j,k+\frac{1}{2}}) - H_\ell(\hat{Q}^{n}_{i,j,k-\frac{1}{2}})$$

$$+ F_\ell(\tilde{Q}^{n+1}_{i+\frac{1}{2},j,k}) - F_\ell(\tilde{Q}^{n+1}_{i-\frac{1}{2},j,k}) + G_\ell(\tilde{Q}^{n+1}_{i,j+\frac{1}{2},k}) - G_\ell(\tilde{Q}^{n+1}_{i,j-\frac{1}{2},k})$$

$$+ H_\ell(\tilde{Q}^{n+1}_{i,j,k+\frac{1}{2}}) - H_\ell(\tilde{Q}^{n+1}_{i,j,k-\frac{1}{2}})] \qquad (3.10)$$

where the $\tilde{Q}^{n+1}_{i+\frac{1}{2},j,k}$, etc, variables are determined in the same way as the $\tilde{Q}^{n}_{i+\frac{1}{2},j,k}$, etc, variables as described below Eq. (3.9) except $\bar{Q}_{i,j,k}$, etc, are used in place of $Q^{n}_{i,j,k}$, etc. The $\hat{Q}^{n}_{i+\frac{1}{2},j,k}$, etc, are determined by

$$\hat{Q}^{n}_{i+\frac{1}{2},j,k} = 2Q^{n}_{i,j,k} - Q^{n}_{i-1,j,k} \qquad \text{if the corresponding } \lambda^1_\xi, \lambda^4_\xi, \text{ or } \lambda^5_\xi \text{ eigenvalue evaluated at } i+\tfrac{1}{2},j,k \text{ is } > 0$$

or

$$\hat{Q}^{n}_{i+\frac{1}{2},j,k} = 2Q^{n}_{i+1} - Q^{n}_{i+2,j,k} \qquad \text{if the corresponding } \lambda^1_\xi, \lambda^4_\xi, \text{ or } \lambda^5_\xi \text{ eigenvalue evaluated at } i+\tfrac{1}{2},j,k \text{ is } \leq 0$$

and similarly for $\hat{Q}^{n}_{i-\frac{1}{2},j,k}$. Again, the same is done for $\hat{Q}^{n}_{i,j\pm\frac{1}{2},k}$ and $Q^{n}_{i,j,k\pm\frac{1}{2}}$ by interrogating the appropriate η or ζ eigenvalues.

Although the algorithm given by Eqs. (3.9) and (3.10) is an extension to three dimensions of that used in Ref. 13 for two dimensions, the interrogation of eigenvalues differs significantly. Three methods were tried in Ref. 13 to handle the computation of flow variables at cell faces when eigenvalues were of different sign on either side of

the cell face. The approach taken in the present scheme is to compute eigenvalues at cell faces rather than at cell centers as illustrated in Fig. 2 on a ζ = constant plane. The difficulty associated with eigenvalues changing sign is thus eliminated. This seems a natural approach because the use of Eq. (2.29) in the finite volume discretized equations (Eq. (3.2)), requires that eigenvalues be known at cell faces. The eigenvalues are computed by averaging the information on either side of a cell face that is necessary for their computation according to Eq. (2.13). Then, depending on the sign of the eigenvalues, the information necessary to compute the remaining terms in the split vectors given by Eq. (2.29) for use in the algorithm given by Eqs. (3.9) and (3.10), is determined by extrapolation from the appropriate direction.

The time step $\Delta\tau_{i,j,k}$ is determined from

$$\Delta\tau_{i,j,k} = \frac{\Delta\tau^{\xi}_{i,j,k}\ \Delta\tau^{\eta}_{i,j,k}\ \Delta\tau^{\zeta}_{i,j,k}}{\Delta\tau^{\xi}_{i,j,k}\ \Delta\tau^{\eta}_{i,j,k} + \Delta\tau^{\xi}_{i,j,k}\ \Delta\tau^{\zeta}_{i,j,k} + \Delta\tau^{\eta}_{i,j,k}\ \Delta\tau^{\zeta}_{i,j,k}} \tag{3.11}$$

where

$$\Delta\tau^{k}_{i,j,k} = \frac{\text{CFL}\ \Delta k}{\max_{\ell} |\lambda^{\ell}_{k}|} \tag{3.12}$$

for k = ξ, η, and ζ. Because the eigenvalues are computed at cell faces rather than cell centers, λ^{ℓ}_{k} is the average of the eigenvalues on cell faces in the k = constant computational planes (where k = ξ, η, or ζ), and ℓ is eigenvalue 4 or 5 because one of these will always have the maximum absolute value. To accelerate convergence for steady-state solutions the maximum allowable time step in each volume is used where CFL $\leq$ 2.

For the computation of the first points inside the computational domain, the scheme is only first order accurate and stable for a CFL of 1. The time steps at these outside points are, therefore, decreased by a factor of 2.

IV. BOUNDARY CONDITIONS

To derive the characteristic variable boundary conditions, the Euler equations need to be cast in characteristic variable form. Therefore, the characteristic variable form of the equations is derived first, followed by the derivation of the boundary conditions for the specific cases of supersonic and subsonic inflow and outflow, and impermeable surfaces.

4.1 Characteristic Variables

Consider the nonconservative form of the Euler equations given by Eq. (2.6). Using Eq. (2.18) in Eq. (2.6), and multiplying Eq. (2.6) on the left by P_k^{-1}, gives

$$P_k^{-1} \frac{\partial q}{\partial \tau} + P_k^{-1} P_k \Lambda_k P_k^{-1} \frac{\partial q}{\partial k} + P_k^{-1} P_m \Lambda_m P_m^{-1} \frac{\partial q}{\partial m} = 0 \qquad (4.1)$$

where $k = \xi$, η, or ζ, and m includes the remaining two curvilinear coordinates out of the set ξ, η, or ζ where $m \neq k$. Therefore, there is a two-term summation on m in the third term in Eq. (4.1). Define the third term in Eq. (4.1) as

$$S_{k,m} = P_k^{-1} P_m \Lambda_m P_m^{-1} \frac{\partial q}{\partial m} \qquad (4.2)$$

with the two-term summation on m understood. Equation (4.1) can be written

$$P_k^{-1} \frac{\partial q}{\partial \tau} + \Lambda_k P_k^{-1} \frac{\partial q}{\partial k} + S_{k,m} = 0 \qquad (4.3)$$

Consider P_k^{-1} to be a constant matrix denoted as $P_{k,o}^{-1}$. Then Eq. (4.3) can be written

$$\frac{\partial(P_{k,o}^{-1}\, q)}{\partial \tau} + \Lambda_k \frac{\partial(P_{k,o}^{-1}\, q)}{\partial k} + S_{k,m} = 0 \qquad (4.4)$$

Defining the characteristic vector, W_k, as

$$W_k = P_{k,o}^{-1} q \qquad (4.5)$$

Eq. (4.4) becomes

$$\frac{\partial W_k}{\partial \tau} + \Lambda_k \frac{\partial W_k}{\partial k} + S_{k,m} = 0 \qquad (4.6)$$

The elements of the characteristic vector, W_k, are called characteristic variables, and are denoted by $w_{k,i}$.

The characteristic variables, $w_{k,i}$, are determined using Eq. (4.5). The vector q is

$$q = J[\rho,\ u,\ v,\ w,\ p]^T$$

and the matrix $P_{k,o}^{-1}$ is given by Eqs. (2.23) where the variables ρ and c (speed of sound) in Eq. (2.23) are denoted ρ_o and c_c to indicate a reference condition. Using q and $P_{k,o}^{-1}$ in Eq. (4.5), the elements of the characteristic vector

$$W_k = (w_{k,1},\ w_{k,2},\ w_{k,3},\ w_{k,4},\ w_{k,5})^T \qquad (4.7)$$

are

$$w_{k,1} = \frac{J}{|\nabla k|}\left[k_x\left(\rho - \frac{p}{c_o^2}\right) + k_z v - k_y w\right] \qquad (4.8a)$$

$$w_{k,2} = \frac{J}{|\nabla k|}\left[k_y\left(\rho - \frac{p}{c_o^2}\right) - k_z u + k_x w\right] \qquad (4.8b)$$

$$w_{k,3} = \frac{J}{|\nabla k|}\left[k_z\left(\rho - \frac{p}{c_o^2}\right) + k_y u - k_x v\right] \qquad (4.8c)$$

$$w_{k,4} = \frac{J}{|\nabla k|}\frac{1}{\sqrt{2}}\left[\frac{p|\nabla k|}{\rho_o c_o} + (k_x u + k_y v + k_z w)\right] \tag{4.8d}$$

$$w_{k,5} = \frac{J}{|\nabla k|}\frac{1}{\sqrt{2}}\left[\frac{p|\nabla k|}{\rho_o c_o} - (k_x u + k_y v + k_z w)\right] \tag{4.8e}$$

The characteristic variables correspond in order to the eigenvalues

$$\lambda_k^1 = k_x u + k_y v + k_z w = \theta_k \tag{4.9a}$$

$$\lambda_k^2 = \theta_k \tag{4.9b}$$

$$\lambda_k^3 = \theta_k \tag{4.9c}$$

$$\lambda_k^4 = \theta_k + c|\nabla k| \tag{4.9d}$$

$$\lambda_k^5 = \theta_k - c|\nabla k| \tag{4.9e}$$

4.2 Characteristic Variable Boundary Conditions

The boundary conditions are derived below assuming locally one-dimensional flow. This assumption is probably better for far field boundary conditions than for boundary conditions applied on or near surfaces. However, numerical experiments using zero pressure gradient, extrapolation, normal pressure gradient, and locally one-dimensional characteristic variable boundary conditions, indicate that similar results can be obtained using any of these four methods for impermeable wall boundary conditions as long as the grid is not extraordinarily coarse. For the computations performed thus far, the locally one-dimensional characteristic variable impermeable wall boundary conditions are to be preferred over the other three methods; hence, this method is developed

below. (Further investigations should be performed without the locally one-dimensional assumption, however.)

By neglecting the ℓ directions in Eq. (4.6) one obtains

$$\frac{\partial W_k}{\partial \tau} + \Lambda_k \frac{\partial W_k}{\partial k} = 0 \tag{4.10}$$

This equation can be written

$$\frac{dW_k}{d\tau} = \frac{\partial W_k}{\partial \tau} + \Lambda_k \frac{\partial W_k}{\partial k} = 0 \tag{4.11}$$

where

$$\frac{dk}{d\tau} = \Lambda_k$$

The eigenvalues, therefore, indicate a direction in computational space. According to Eq. (4.11) one particular eigenvalue is associated with one particular characteristic variable. Each eigenvalue, λ_k^i, indicates the direction across the k = constant computational surface that information contained in the associated characteristic variable, $w_{k,i}$, propagates. This result is the basis for determining the boundary conditions referred to here as characteristic variable boundary conditions.

Boundary conditions are now developed for the following five specific cases

1. supersonic inflow
2. supersonic outflow
3. subsonic inflow
4. subsonic outflow
5. impermeable surface

Supersonic Inflow

This is a situation where all eigenvalues have the same sign. Because flow is coming into the compurational domain, all flow variables are specified.

Supersonic Outflow

This is another situation where all eigenvalues have the same sign. Because flow is leaving the computational domain all flow variables at the boundary must be obtained from the solution in the computational domain. All flow variables are extrapolated from inside the computational domain to the boundary.

Subsonic Inflow

This situation is characterized by four eigenvalues of the same sign and one of differing sign. For the subsonic inflow case shown in Fig. 3a with the flow in the direction of increasing computational coordinate k, the first four eigenvalues are positive and the fifth is negative. For the subsonic inflow case shown in Fig. 3b with the flow in the direction of decreasing computational coordinate k, the first three and fifth eigenvalues are negative and the fourth eigenvalue is positive. For a totally general three-dimensional code either situation in Fig. 3 could occur. Each possiblity in Fig. 3 is taken into account in the following derivation. Using the characteristic variables given by Eqs. (4.8) one obtains

$$[k_x(\rho - \frac{p}{c_o^2}) + k_z v - k_y w]_a = [k_x(\rho - \frac{p}{c_o^2}) + k_z v - k_y w]_b \quad (4.12a)$$

$$[k_y(\rho - \frac{p}{c_o^2}) - k_z u + k_x w]_a = [k_y(\rho - \frac{p}{c_o^2}) - k_z u + k_x w]_b \quad (4.12b)$$

$$[k_z(\rho - \frac{p}{c_o^2}) + k_y u - k_x v]_a = [k_z(\rho - \frac{p}{c_o^2}) + k_y u - k_x v]_b \qquad (4.12c)$$

$$[\frac{p|\nabla k|}{\rho_o c_o} \pm (k_x u + k_y v + k_z w)]_a = [\frac{p|\nabla k|}{\rho_o c_o} \pm (k_x u + k_y v + k_z w)]_b \qquad (4.12d)$$

$$[\frac{p|\nabla k|}{\rho_o c_o} \mp (k_x u + k_y v + k_z w)]_\ell = [\frac{p|\nabla k|}{\rho_o c_o} \mp (k_x u + k_y v + k_z w)]_b \qquad (4.12e)$$

where the plus signs in Eq. (4.12d) and the negative signs in Eqs. (4.12e) refer to the situation in Fig. 3a, and the other sign option refers to the situation in Fig. 3b. The subscript a refers to approaching the boundary, subscipt b refers to the boundary, and subscript ℓ refers to leaving the boundary (see Fig. 3). Note from the equations for k_x, k_y, and k_z given below Eq. (2.2) that the products Jk_x, Jk_y, and Jk_z are components of area vectors. The computer code actually uses these components of cell surface areas, and because the boundary of interest in Eqs. (4.12) is the cell face containing the boundary point b, the area vector components of interest correspond to this cell face. The metrics at points a and ℓ are taken to be the same as those at point b, and the coefficients of the bracket terms in Eqs. (4.8) are not carried through the manipulation of the equations. The linearization point o is taken to be on the boundary.

Equations (4.12d) and (4.12e) can be combined to obtain

$$p_b = \tfrac{1}{2}\{p_a + p_\ell \pm \rho_o c_o[\tilde{k}_x(u_a - u_\ell) + \tilde{k}_y(v_a - v_\ell) + \tilde{k}_z(w_a - w_\ell)]\} \qquad (4.13a)$$

where $\tilde{k}_x$, $\tilde{k}_y$, and $\tilde{k}_z$ are defined by Eqs. (2.15). Equations (4.12a), (4.12b), (4.12c), and (4.12d) can be solved for the four remaining unknown boundary values, giving

$$\rho_b = \rho_a + \frac{p_b - p_a}{c_o^2} \qquad (4.13b)$$

$$u_b = u_a \pm \tilde{k}_x \frac{p_a - p_b}{\rho_o c_o} \qquad (4.13c)$$

$$v_b = v_a \pm \tilde{k}_y \frac{p_a - p_b}{\rho_o c_o} \qquad (4.13d)$$

$$w_b = w_a \pm \tilde{k}_z \frac{p_a - p_b}{\rho_o c_o} \qquad (4.13e)$$

The plus sign option in Eqs. (4.13) refers to the computational coordinate and inflow situation depicted in Fig. 3a, and the negative sign option refers to Fig. 3b. There is no sign option in Fig. (4.13b). Note that these signs correspond to the sign of the first three eigenvalues, and hence this is a means of writing the code for general applications with arbitrary orientation of the computation coordinates. The point a is outside the computational domain, point b is on the computational boundary, and point ℓ is inside the computational domain.

Subsonic Outflow

This situation is also characterized by four eigenvalues of the same sign and one of opposite sign. The development of subsonic outflow boundary conditions is similar to that for subsonic inflow, and Fig. 3 can be used again for illustration. However, for subsonic outflow only one characteristic variable is specified and four are determined from information inside the computational domain, whereas, for subsonic inflow four characteristic variables were specified and one was determined from information inside the computational domain. Using the characteristic variables given by Eqs. (4.8), and the signs of the eigenvalues given by Eqs. (4.9) for the situations in Fig. 3, one obtains a set of

equations identical to Eqs. (4.12). Note, however, that although the equations are identical, point a is now inside the computational domain and point ℓ is outside the computational domain; whereas, just the opposite was true for subsonic inflow.

Because the equations for subsonic outflow are the same as Eqs. (4.12), they have the same formal solution. However, because one characteristic variable is specified, the resulting boundary conditions differ somewhat from the subsonic inflow boundary conditions. Consider Eq. (4.12e). By specifying that the outflow is straight, then $p_b = p_\ell$ according to Eqs. (4.12e). The remaining four equations can be solved for the remaining four variables giving

$$p_b = p_\ell \tag{4.14a}$$

$$\rho_b = \rho_a + \frac{p_b - p_a}{c_o^2} \tag{4.14b}$$

$$u_b = u_a \pm \tilde{k}_x \frac{p_a - p_b}{\rho_o c_o} \tag{4.14c}$$

$$v_b = v_a \pm \tilde{k}_y \frac{p_a - p_b}{\rho_o c_o} \tag{4.14d}$$

$$w_b = w_a \pm \tilde{k}_z \frac{p_a - p_b}{\rho_o c_o} \tag{4.14e}$$

The plus and minus signs have the same meaning here as for Eqs. (4.13). For external flow computations, p_ℓ could be the ambient static pressure, p_∞.

Impermeable Surface

For a boundary across which there is no flow the first three eigenvalues given by Eq. (4.9) are zero, the fourth is positive, and the fifth is negative. One condition must, therefore, be specified. The condition specified is that there is no flow across the boundary. The following relations among the characteristic variables are used to determine the boundary conditions

$$[k_x(\rho - \frac{p}{c_o^2}) + k_z v - k_y w]_b = [k_x(\rho - \frac{p}{c_o^2}) + k_z v - k_y w]_r \qquad (4.15a)$$

$$[k_y(\rho - \frac{p}{c_o^2}) - k_z u + k_x w]_b = [k_y(\rho - \frac{p}{c_o^2}) - k_z u + k_x w]_r \qquad (4.15b)$$

$$[k_z(\rho - \frac{p}{c_o^2}) + k_y u - k_x v]_b = [k_z(\rho - \frac{p}{c_o^2}) + k_y u - k_x v]_r \qquad (4.15c)$$

$$[k_x u + k_y v + k_z w]_b = 0 \qquad (4.15d)$$

$$[\frac{p|\nabla k|}{\rho_o c_o} \mp (k_x u + k_y v + k_z w)]_b = [\frac{p|\nabla k|}{\rho_o c_o} \mp (k_x u + k_y v + k_z w)]_r \qquad (4.15e)$$

The subscript r refers to a reference value, which is selected as the center of the first cell from the boundary. The minus and plus signs in Eq. (4.15e) correspond to the location of the point r. If the point r is in the positive k direction from the boundary then the minus sign is used in Eq. (4.15e), and if it is in the minus direction then the plus sign is used.

Finite volume codes only require the pressure at an impermeable boundary and consequently Eqs. (4.15a), (4.15b), and (4.15c) are not needed. However, to facilitate the handling of points near boundaries and aid in code vectorization, phantom points are used in the present version of the code. The use of phantom points requires information of variables other than pressure to ensure, for example, zero flow across an impermeable boundary. Such information can be obtained from Eqs. (4.15).

Equations (4.15d) and (4.15e) can be solved for p_b. Equations (4.15a) - (4.15d) can then be solved for the remaining four variables. The solution of Eqs. (4.15) is

$$p_b = p_r \mp \rho_o c_o (\tilde{k}_x u_r + \tilde{k}_y v_r + \tilde{k}_z w_r) \tag{4.16a}$$

$$\rho_b = \rho_r + \frac{p_b - p_r}{c_o^2} \tag{4.16b}$$

$$u_b = u_r - \tilde{k}_x (\tilde{k}_x u_r + \tilde{k}_y v_r + \tilde{k}_z w_r) \tag{4.16c}$$

$$v_b = v_r - \tilde{k}_y (\tilde{k}_x u_r + \tilde{k}_y v_r + \tilde{k}_z w_r) \tag{4.16d}$$

$$w_b = w_r - \tilde{k}_z (\tilde{k}_x u_r + \tilde{k}_y v_r + \tilde{k}_z w_r) \tag{4.16e}$$

where the point r is the center of the first cell from the boundary and the minus sign in Eq. (4.16a) is used if r is in the positive k direction from the boundary, and the plus sign is used if r is in the negative k direction from the boundary.

4.3 Phantom Points

Phantom points are denoted by the subscript p. The points are obtained from the relations

$$p_p = 2p_b - p_{in} \tag{4.17a}$$

$$\rho_p = 2\rho_b - \rho_{in} \tag{4.17b}$$

$$u_p = 2u_b - u_{in} \tag{4.17c}$$

$$v_p = 2v_b - v_{in} \tag{4.17d}$$

$$w_p = 2w_b - w_{in} \tag{4.17e}$$

where the subscript in refers to the center of the first cell inside the computational domain and can be any of the points a, ℓ, or r used in this section. For example, the phantom points for an impermeable surface are

$$p_p = p_r \mp 2\rho_o c_o(\tilde{k}_x u_r + \tilde{k}_y v_r + \tilde{k}_z w_r) \tag{4.18a}$$

$$\rho_p = \rho_r + \frac{2(p_b - p_r)}{c_o^2} \tag{4.18b}$$

$$u_p = u_r - 2\tilde{k}_x(\tilde{k}_x u_r + \tilde{k}_y v_r + \tilde{k}_z w_r) \tag{4.18c}$$

$$v_p = v_r - 2\tilde{k}_y(\tilde{k}_x u_r + \tilde{k}_y v_r + \tilde{k}_z w_r) \tag{4.18d}$$

$$w_p = w_r - 2\tilde{k}_z(\tilde{k}_x u_r + \tilde{k}_y v_r + \tilde{k}_z w_r) \tag{4.18e}$$

The velocity vector components are the same as those used by Jacocks and Kneile (Ref. 14).

V. RESULTS

The computer program written to solve the three-dimensional unsteady Euler equations is referred to as the SKOAL code. SKOAL is an acronym for nothing.

To investigate the results of this code a numerical solution was obtained for the ONERA M6 wing at $M_\infty = 0.84$ and $\alpha = 3.06°$. The pressure distribution is shown in Fig. 4. This solution is compared to a solution from the FL057 code in Fig. 5. Identical 96x16x16 meshes were used for both solutions in Fig. 5. The major difference between the two solutions occurs in the outboard region of the wing. More detailed comparisons between the solutions, including comparisons with experimental data (Ref. 15), are given in Fig. 6. Comparisons of spanwise distributions of lift and drag are given in Fig. 7. The FL057 code gives a 4% higher value of lift to drag ratio than the SKOAL code.

The number of supersonic points (NSUP) is sometimes used as a crude indication of convergence. The FL057 solution was obtained by first using a 48x8x8 grid and then using this crude grid solution as initial conditions for the 96x16x16 grid solution. Hence the NSUP corresponding to an impulsive start for the 96x16x16 grid was not available from the FL057 code for comparison with the SKOAL code. In order to compare the NSUP history between the two codes, a 48x8x8 grid solution was obtained using the SKOAL code. These results are presented in Fig. 8. The FL057 code is stable for a CFL of 2.8 using a four-stage Runge-Kutta scheme, whereas, the SKOAL code is stable for a CFL of 2.0 using the predictor-corrector scheme. It is interesting to note

that the number of cycles required for the NSUP to become constant using FL057 is 246, whereas, the number of cycles required for the NSUP to become constant using SKOAL is 325. The ratio of these two numbers is essentially the inverse ratio of CFL numbers. Another way of looking at this is to note that FL057 passes through a flux balance routine four times during each cycle, whereas SKOAL passes through a flux balance routine three time during each cycle. A comparison of the ratio of the NSUP to the final number of NSUP (denoted as NSUP/$(NSUP)_c$) as a function of flux balances is given in Fig. 9. Based on the number of flux balances required to reach steady state for this solution these methods are operating identically. However, one pass through a dissipation routine (which is similar in terms of computer resources to an extra pass through the flux balance routine) is required in the FL057 code which is not required in the SKOAL code because no additional dissipation terms were included. The important comparison, however, is the number of computer resource units required to reach steady state. This depends on the coding, vectorization, storage, etc., of each code on the same machine. Such a comparison cannot presently be made. As the codes now stand, the FL057 code is probably at least twice as fast as the SKOAL code per cycle. However, based on Fig. 9, it is anticipated that the SKOAL code can be improved.

Numerous other results have been obtained using the SKOAL code for various two-and three-dimensional geometries, and for subsonic, transonic, and supersonic flow. The ONERA wing, however, is the only solution obtained thus far that can be compared to another Euler code solution for which the same mesh was used.

VI. CONCLUDING REMARKS

A method was presented for solving the three-dimensional unsteady Euler equations based on flux vector splitting. The equations were cast in curvilinear coordinates and a finite volume discretization was used for handling arbitrary geometries. The discretized equations were solved using an explicit upwind second-order predictor-corrector scheme that is stable for a CFL of 2. No additional dissipation terms were included in the scheme. Local time stepping was used to accelerate convergence for steady-state problems. Characteristic variable boundary conditions were developed and applied in the far field and at impermeable surfaces. Numerical results were obtained and compared with results from the FL057 code and experimental data for the ONERA M6 wing at $M_\infty = 0.84$ and $\alpha = 3.06°$.

REFERENCES

1. Whitfield, D. L. and Jameson, A., "Three-Dimensional Euler Equation Simulation of Propeller-Wing Interaction in Transonic Flow," AIAA Paper 83-0236, January 1983.

2. Jameson, A., Schmidt, W., and Turkel, E., "Numerical Solutions of the Euler Equations by Finite Volume Methods Using Runge Kutta Time Stepping Schemes," AIAA Paper No. 81-1259, June 1981.

3. Schmidt, W., Jameson, A., and Whitfield, D. L., "Finite-Volume Solutions to the Euler Equations in Transonic Flow," Journal of Aircraft, Vol. 20, No. 2, February 1983, pp. 127-133.

4. Swafford, T. W., "Three-Dimensional, Time-Dependent, Compressible, Turbulent, Integral Boundary-Layer Equations in General Curvilinear Coordinates and Their Numerical Solution," Ph.D. Dissertation, Mississippi State University, August, 1983.

5. Steger, J. L. and Warming, R. F., "Flux Vector Splitting of The Inviscid Gasdynamic Equations with Application to Finite-Difference Methods," Journal of Computational Physics, Vol. 40, 1981, pp. 263-293.

6. Warming, R. F., Beam, R. M., and Hyett, B. J., "Diagonalization and Simultaneous Symmetrization of the Gas-Dynamic Matrices," Mathematic of Computation, Vol. 20, No. 132, October 1975, pp. 1037-1045.

7. Pulliam, T. H. and Chaussee, D. S., "A Diagonal Form of an Implicit Approximate-Factorization Algorithm," Journal of Computational Physics, Vol. 39, 1981, pp. 347-363.

8. Nobel, B. and Daniel, J. W., Applied Linear Algebra. Second Edition, Prentice-Hall, Inc., Englewood Cliffs, New Jersey, 1977.

9. Olmsted, J. M. H., Real Variables. Appleton-Century-Crofts, Inc., New York, 1959.

10. Reklis, R. P. and Thomas, P. D. "Shock-Capturing Algorithm for the Navier-Stokes Equations," AIAA Journal, Vol. 20, No. 9, September 1982, pp. 1212-1218.

11. Thomas, P. D. and Lombard, C. K., "Geometric Conservation Law and Its Application to Flow Computations on Moving Grids," AIAA Journal Vol. 17, No. 10, October 1979, pp. 1030-1037

12. Warming, R. F. and Beam, R. M., "Upwind Second-Order Difference Schemes and Applications in Aerodynamic Flows," AIAA Journal, Vol. 14, No. 9, September 1976, pp. 1241-1249.

13. Deese, J. E., "Numerical Experiments with the Split-Flux-Vector Form of the Euler Equations," AIAA Paper No. 83-0122, January 1983.

14. Jacocks, J. L. and Kneile, K. R., "Computation of Three-Dimensional Time-Dependent Flow Using the Euler Equations," AEDC-TR-80-49, July, 1981.

15. Schmitt, V. and Charpin, F., "Pressure Distriubtions on the ONERA M6-Wing at Transonic Mach Numbers," Experimental Data Base for Computer Program Assessment, AGARD AR-138, 1979.

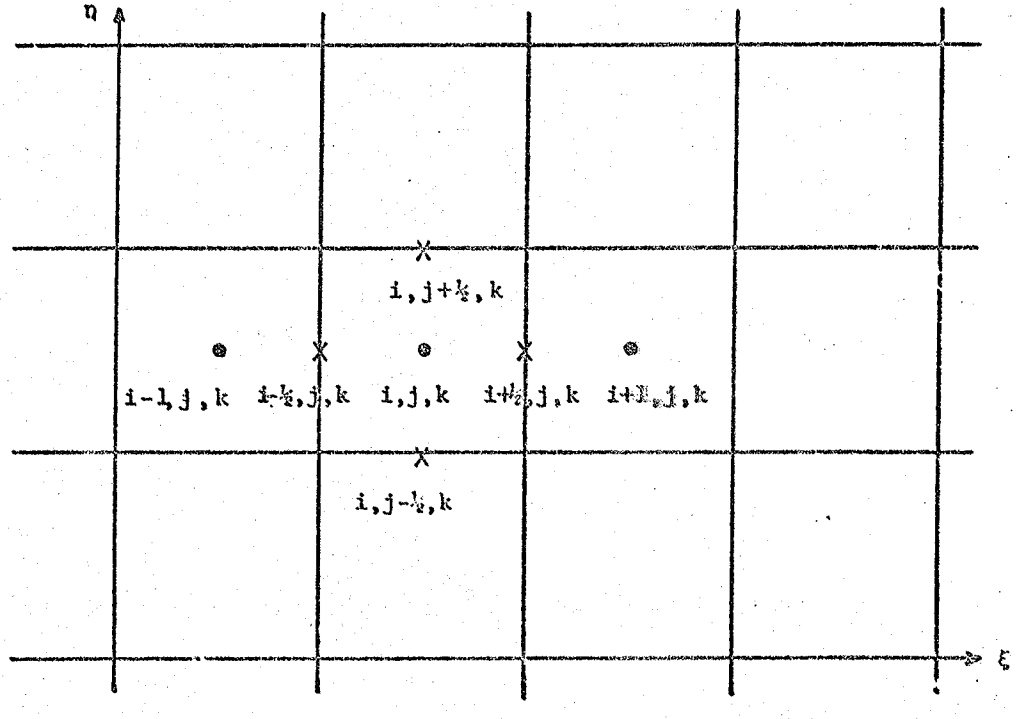

ζ = CONSTANT PLANE

Fig. 1 Computational Grid.

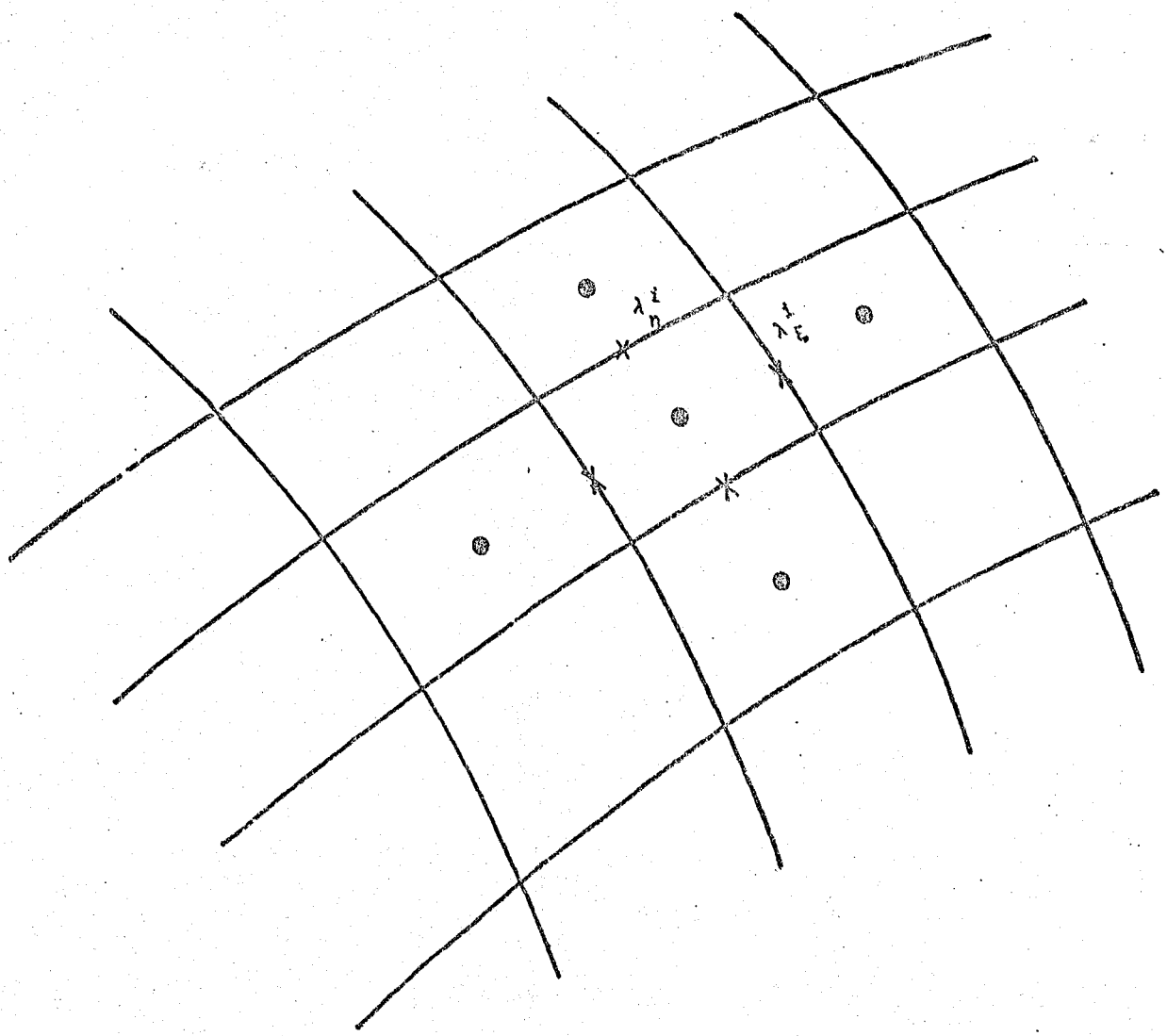

Fig. 2 Location of Interrogated Eigenvalues.

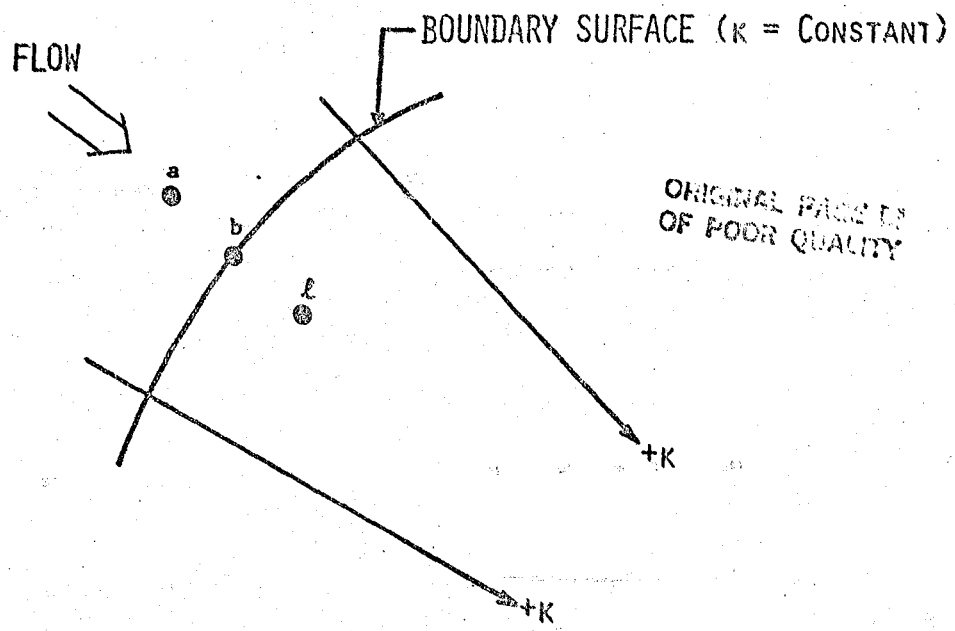

A. Flow in Direction of +k.

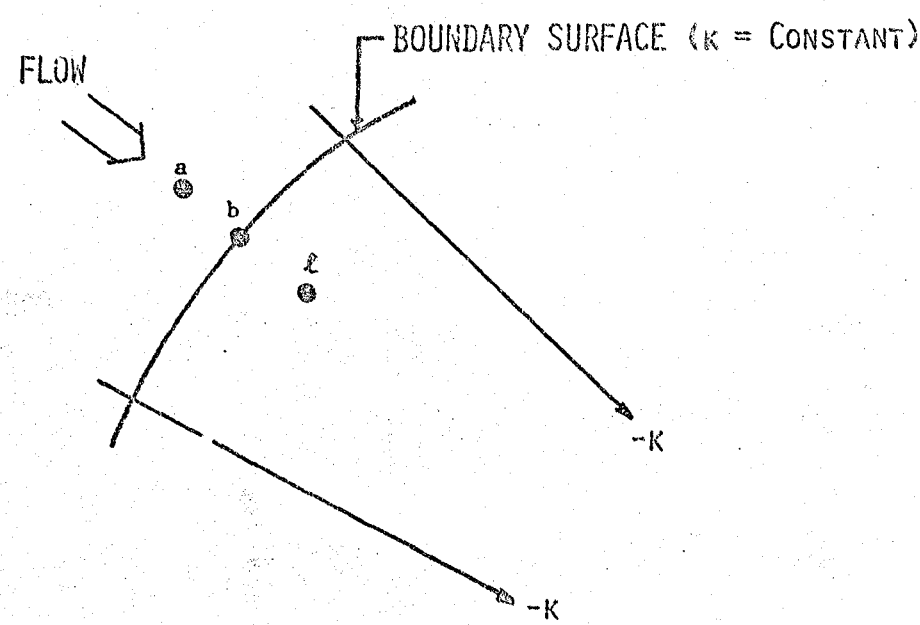

B. Flow in Direction of -k.

Fig. 3 Computational Coordinates Schematic for Characteristic Variable Boundary Conditions.

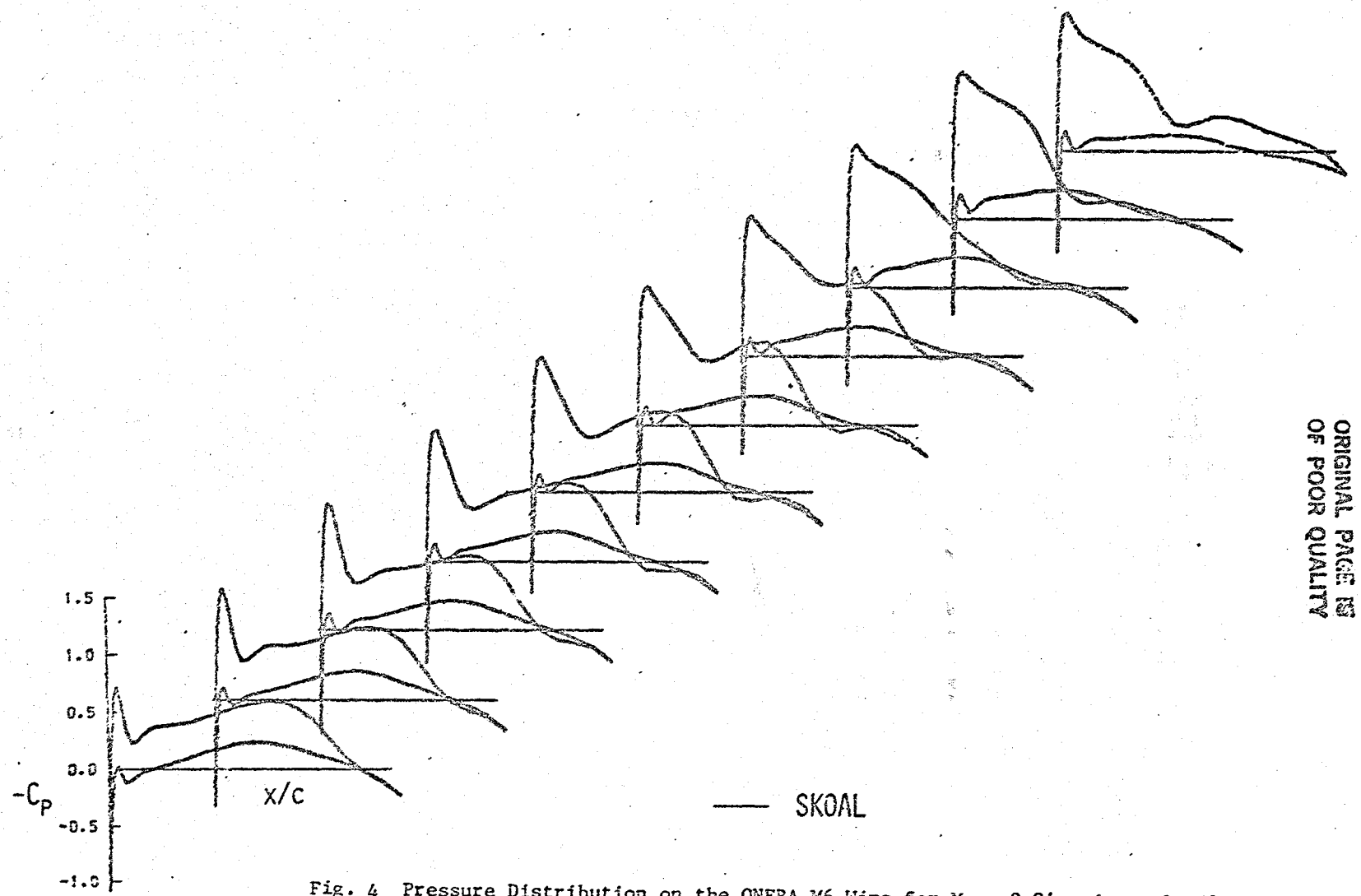

Fig. 4 Pressure Distribution on the ONERA M6 Wing for $M_\infty = 0.84$ and $\alpha = 3.06°$.

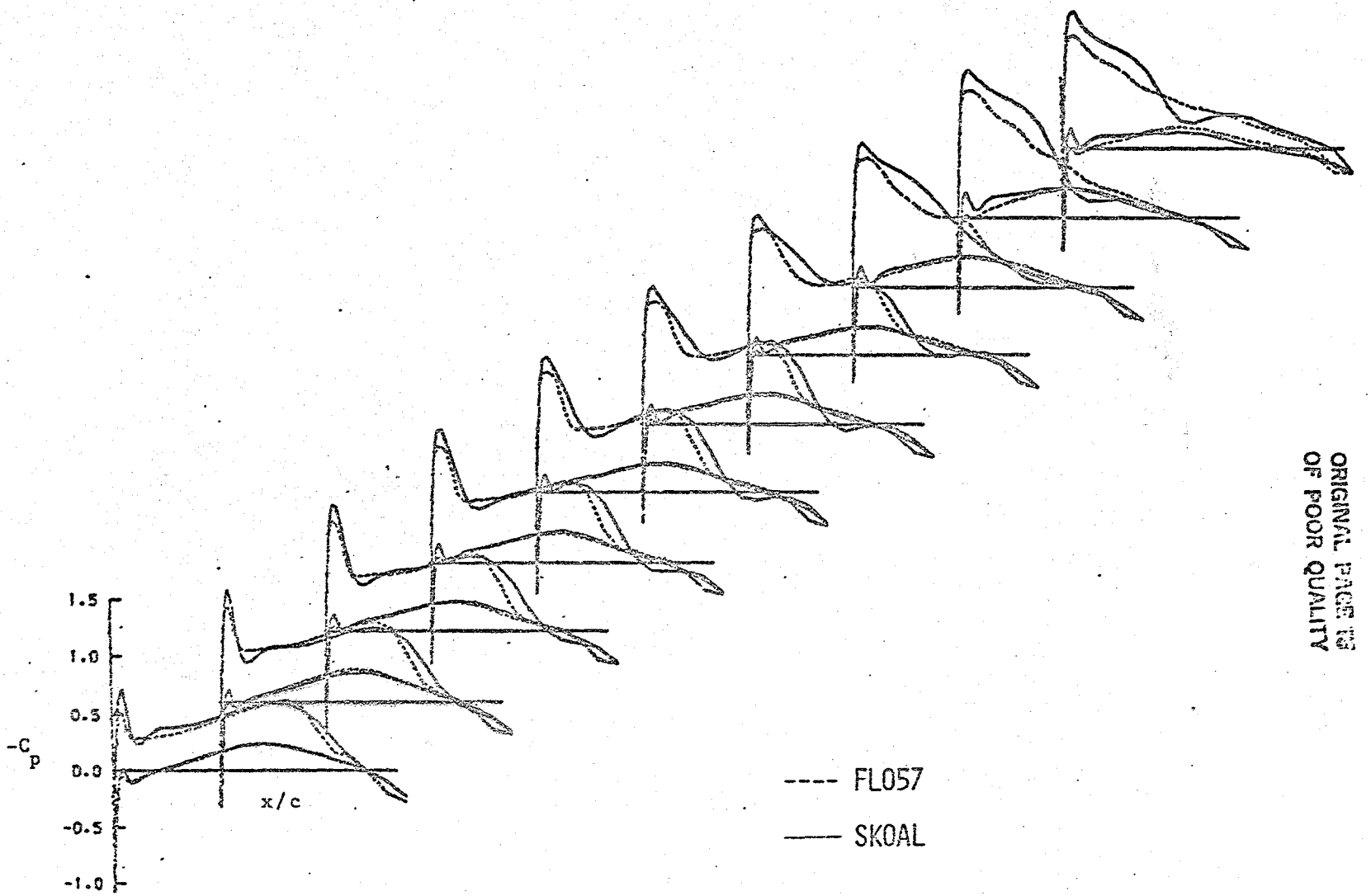

Fig. 5 Pressure Distribution Comparisons on the ONERA M6 Wing for $M_\infty = 0.84$ and $\alpha = 3.06°$.

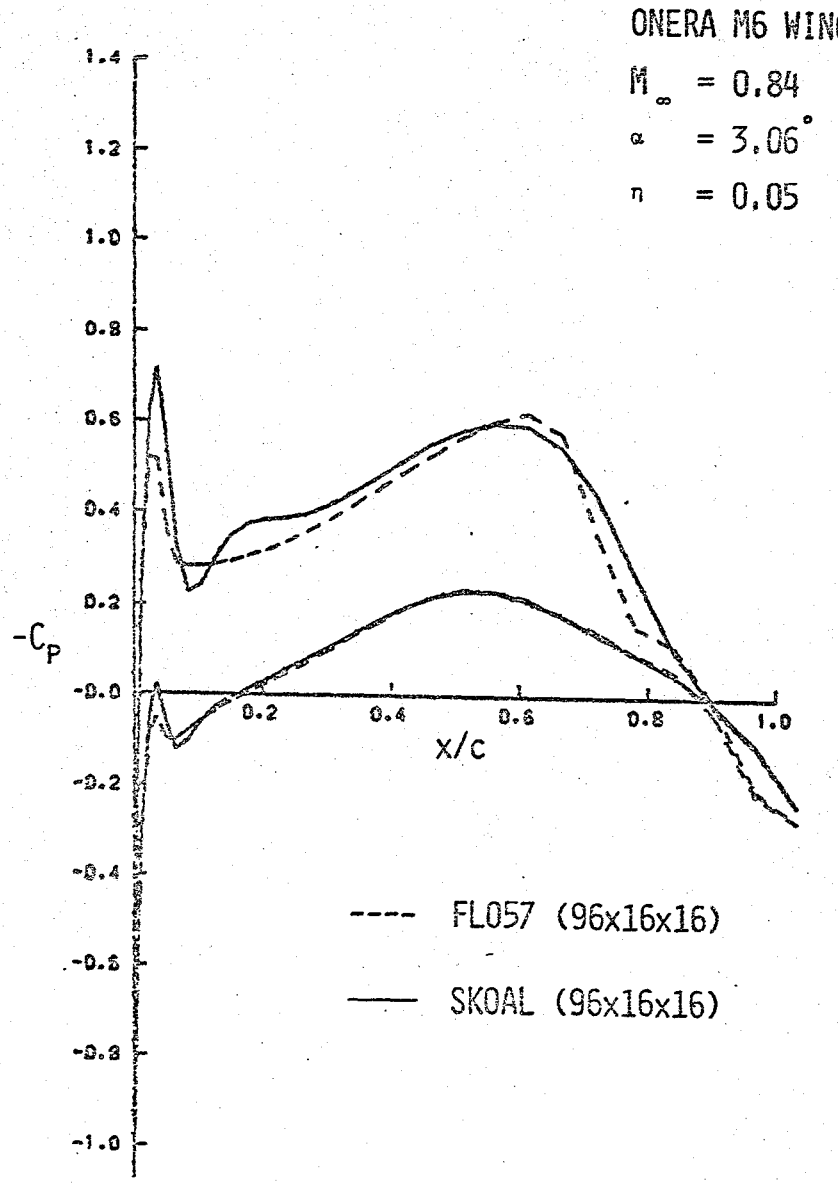

Fig. 6 Numerical and Experimental Pressure Distributions at Various Span Locations.

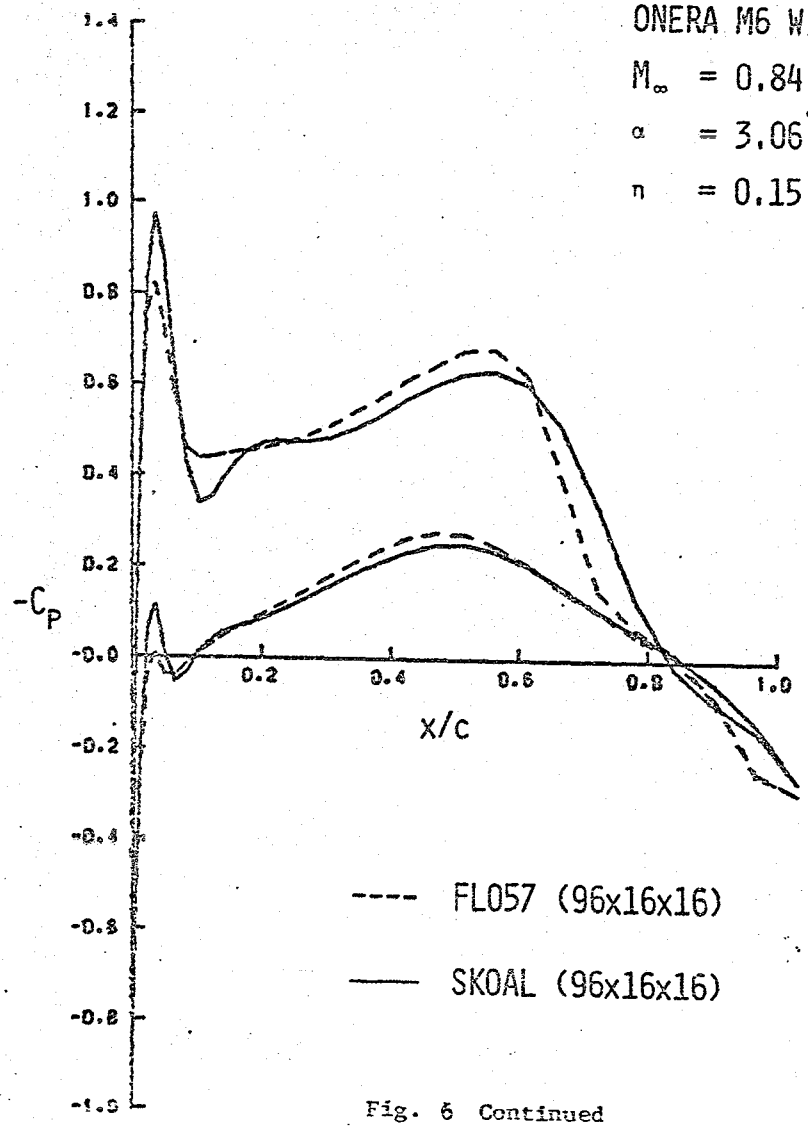

Fig. 6 Continued

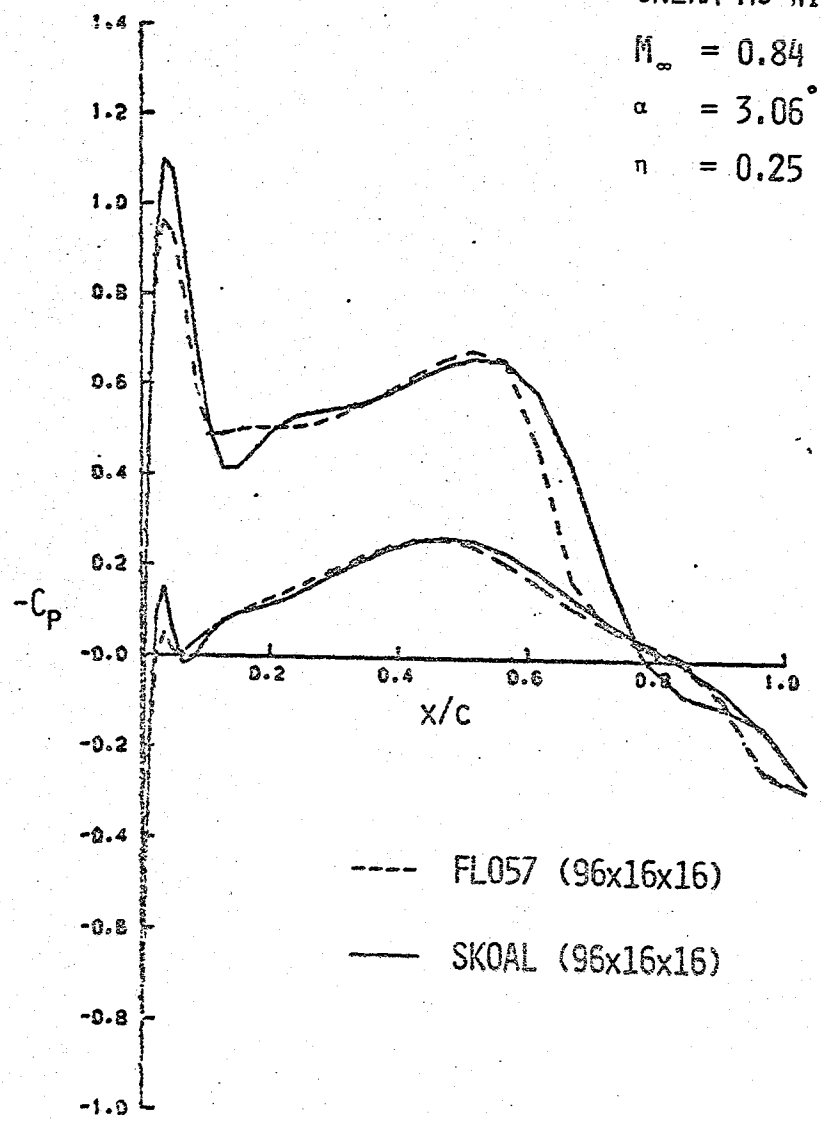

Fig. 6 Continued

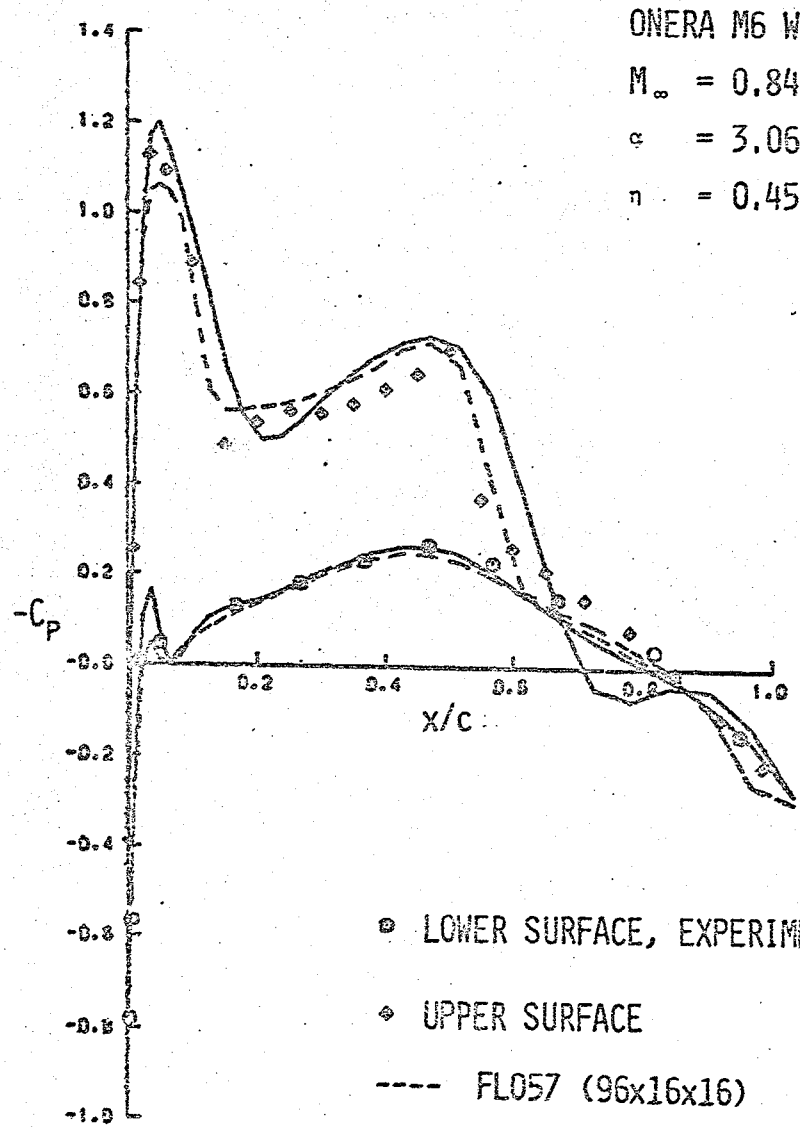

Fig. 6 Continued

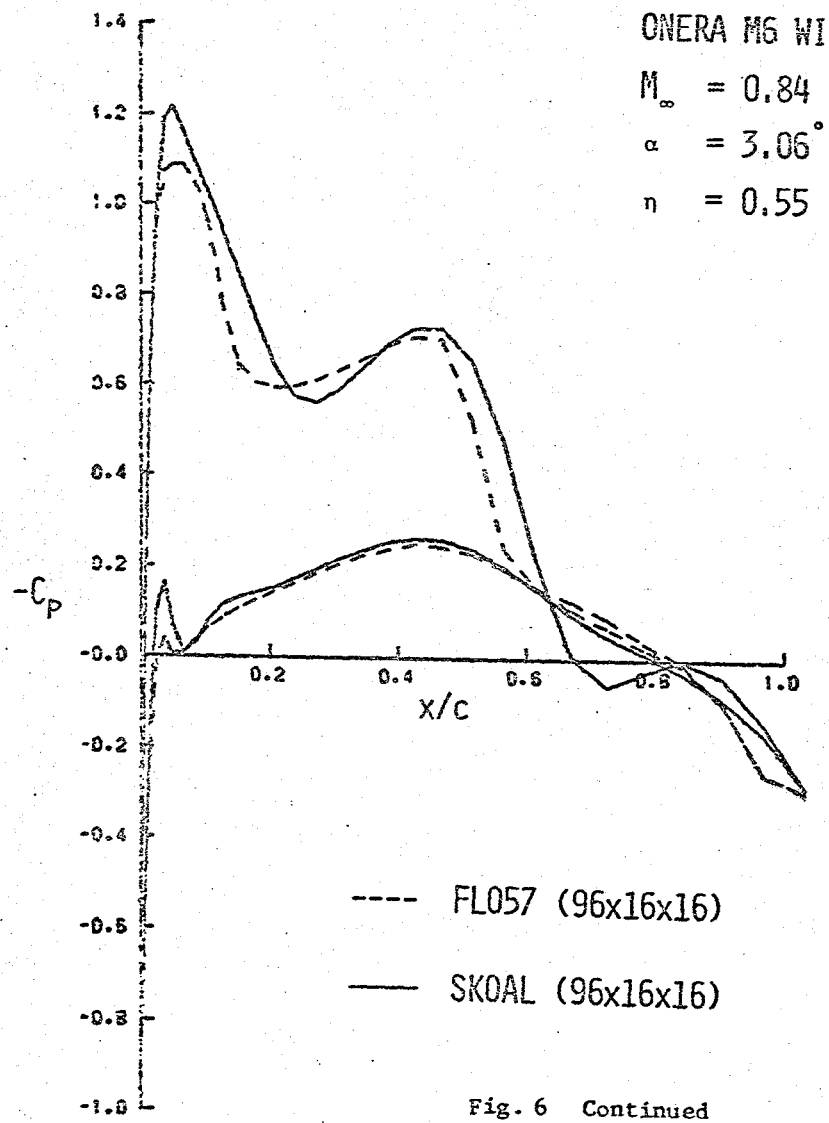

Fig. 6 Continued

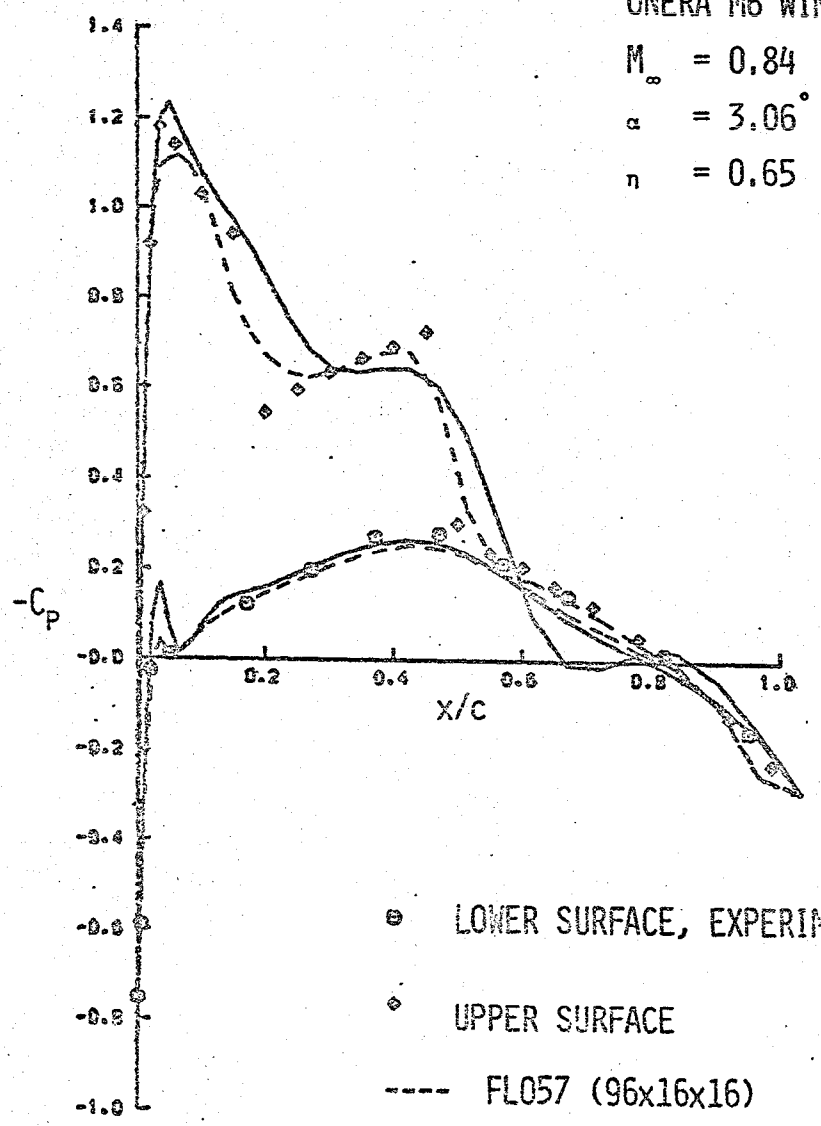

Fig. 6 Continued

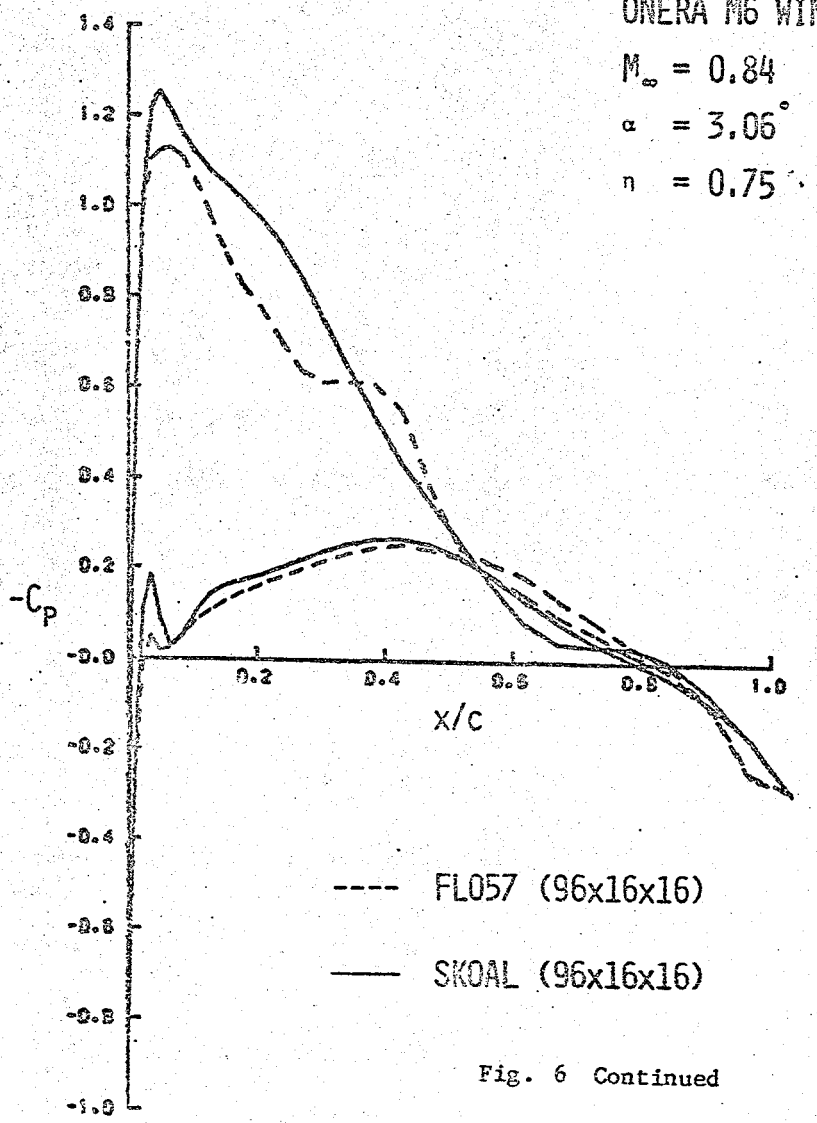

Fig. 6 Continued

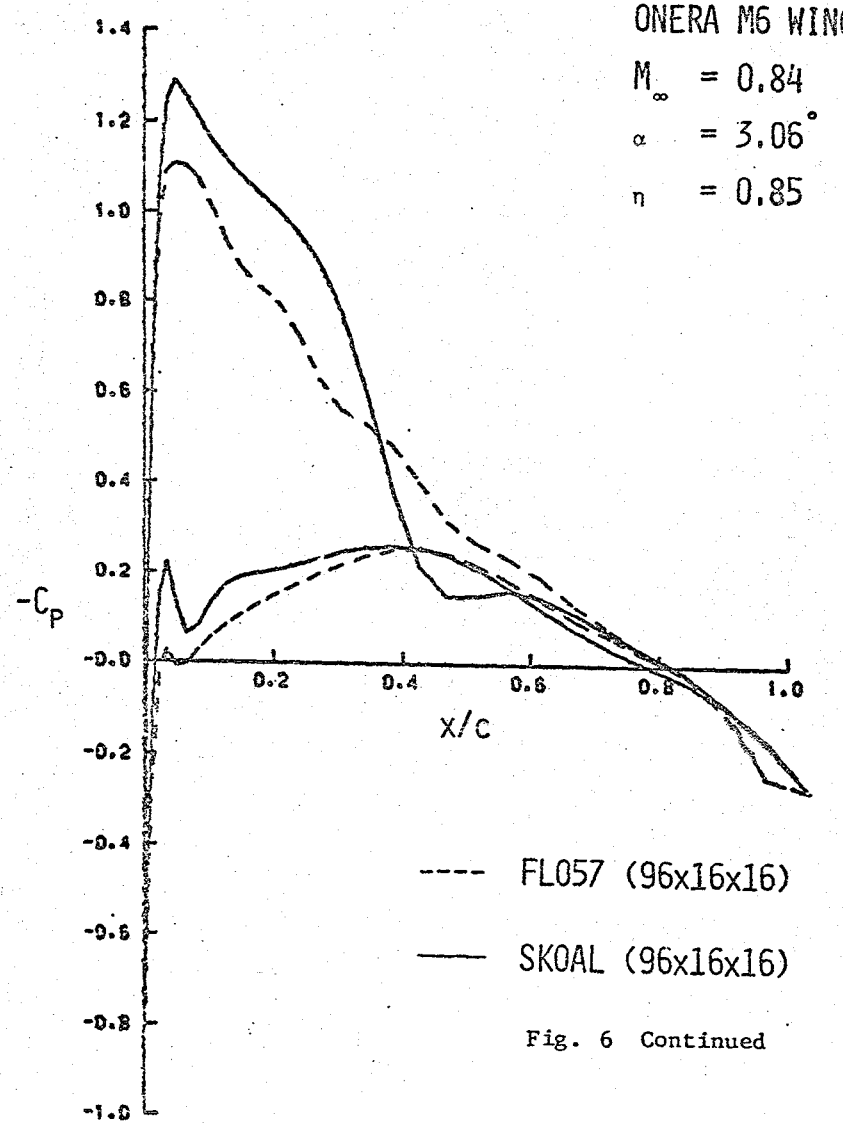

Fig. 6 Continued

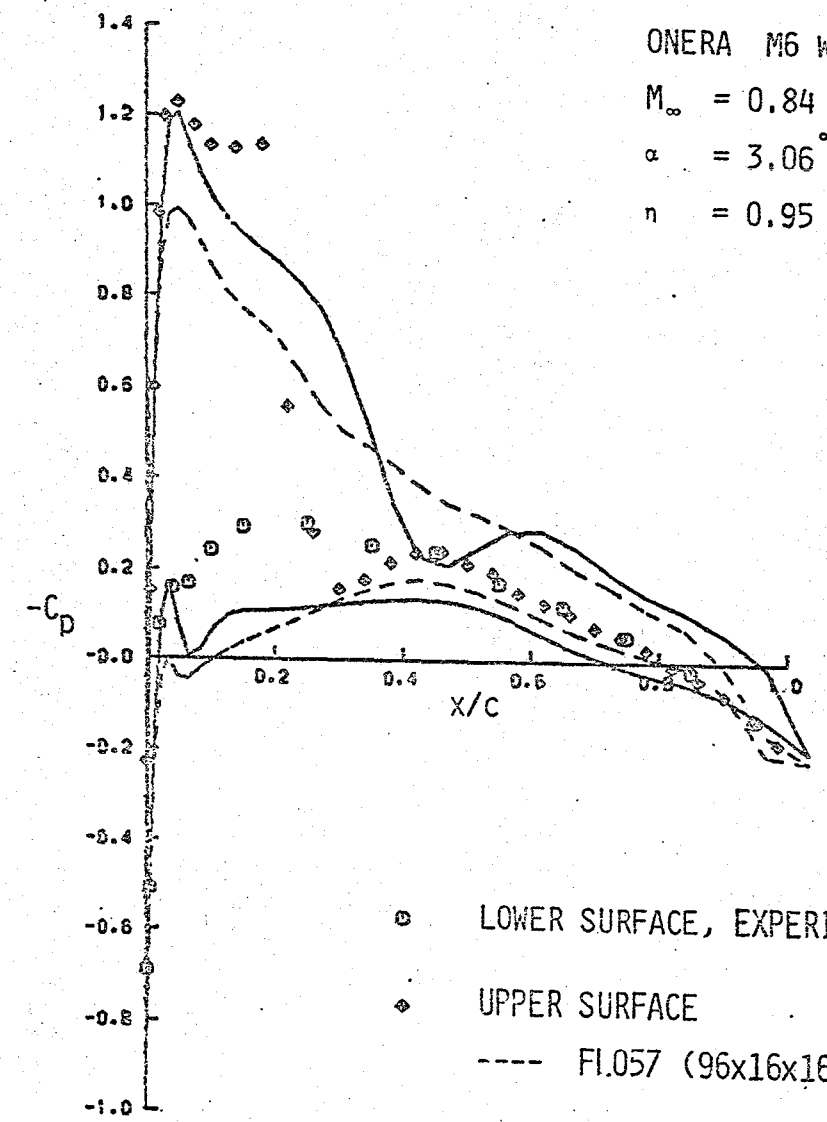

Fig. 6 Concluded

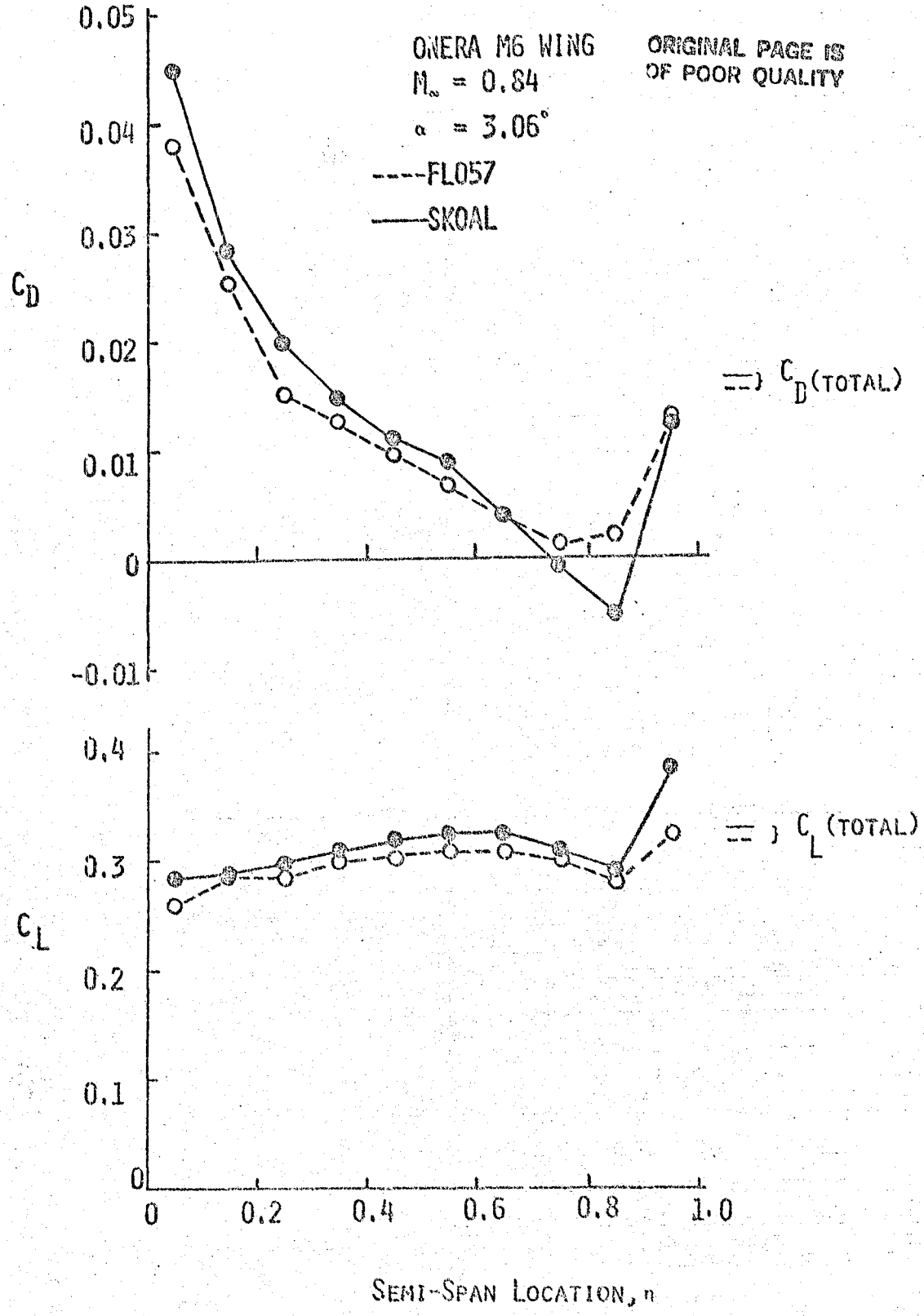

Fig. 7 Spanwise Lift and Drag Distribution.

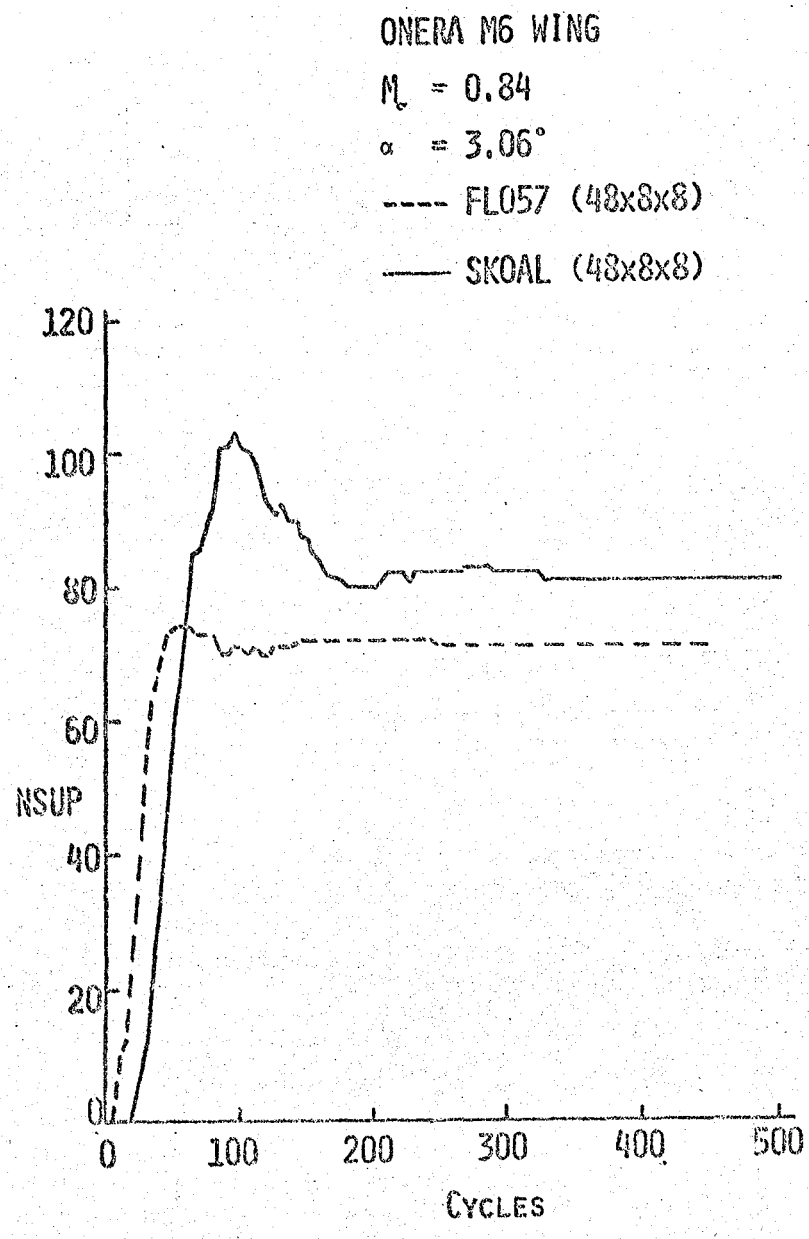

Fig. 8. Number of Supersonic Points (NSUP) as a Function of Cycles.

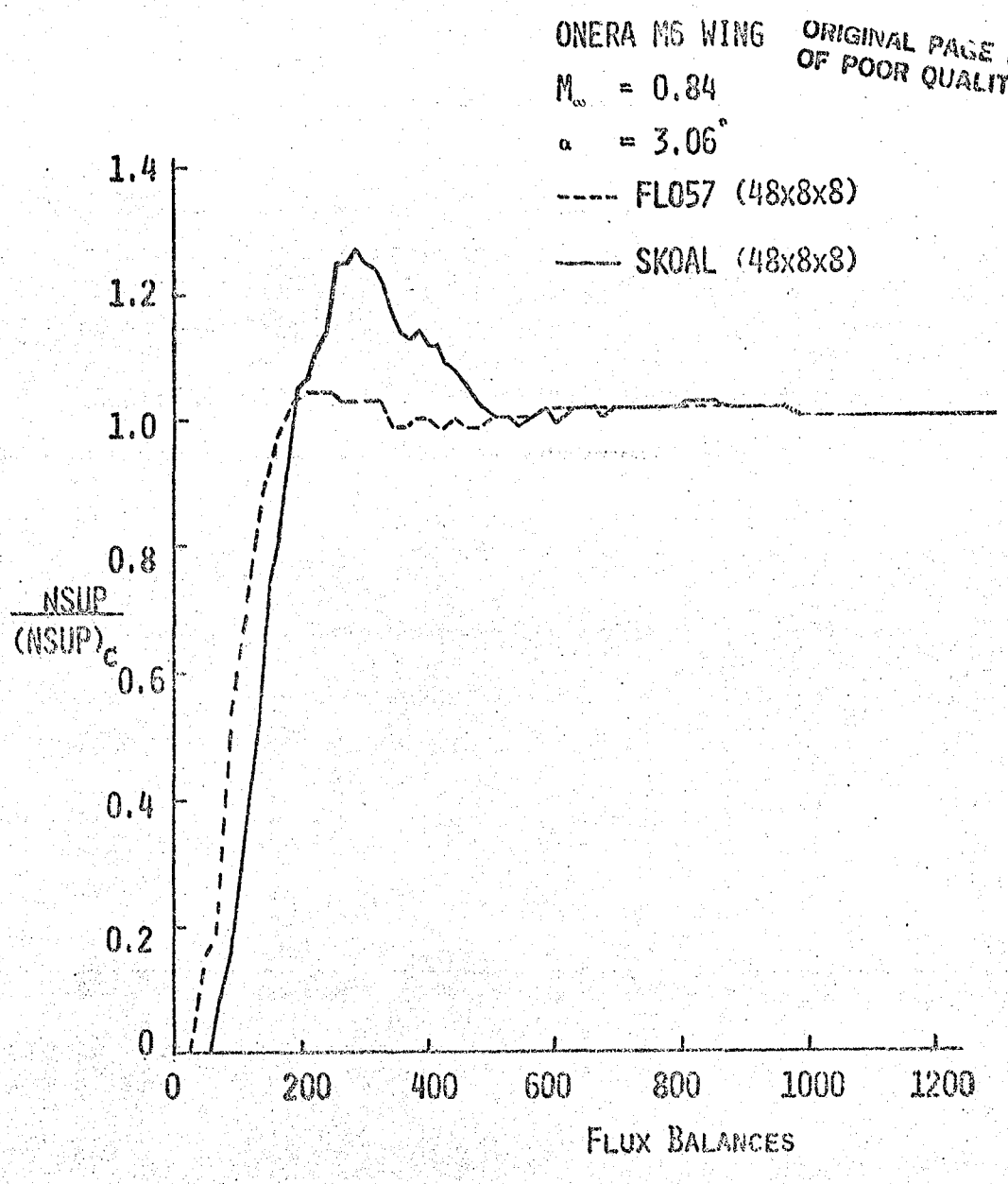

Fig. 9 Number of Supersonic Points (NSUP) as a Function of Flux Balances.

End of Document